

1 **Global-Scale Characterization of Streamflow Extremes**

2 Sai Kiran Kuntla¹, Manabendra Saharia¹, Pierre Kirstetter²

3
4 ¹Department of Civil Engineering, Indian Institute of Technology Delhi, New Delhi 110016,
5 India

6 ²University of Oklahoma, Norman, Oklahoma, 73019, United States

7
8
9
10
11
12
13 Submitted for publication in *Journal of Hydrology*

14
15
16
17
18

This manuscript has been submitted for publication in Journal of Hydrology. Please note that, this manuscript is currently under review. Subsequent versions of this manuscript may have slightly different content. If accepted, the final version of this manuscript will be available via the ‘published version of this preprint is available.’ DOI link on the top of this webpage.

19

20

Abstract:

The increasing risk of floods across the globe needs focused attention because of the extensive damage to human lives and economy. A comprehensive understanding of its causative factors is of vital importance. Yet catchment characterization studies are generally limited to case studies or regional domains. A comprehensive global characterization is currently unavailable, which requires collecting and collating a large number of datasets over vast areas. This study embraces large-sample data-driven science as a new paradigm to characterize streamflow extremes by utilizing global datasets of physiographic explanatory variables that could explain various facets of extreme streamflows. Along with the spatial and temporal variations of high streamflow extremes, their correlation with various catchment characteristics such as geomorphology, meteorology, climatology, landcover, lithology, etc. were examined. The multidimensional relationships between the streamflow extremes and catchment characteristics were modeled using a Random Forest approach and combined with an interpretable machine learning framework to identify the most dominant factors in varying climate classes. Interpretation with SHAP (SHapley Additive exPlanations) reveals that meteorological variables are the most influential variables across the climatic classes. However, the variables and their influences change among different climatic classes. Moreover, different geomorphological variables come into dominance across climatic classes (such as basin relief in warm temperate and drainage texture in arid climates). Overall, the insights from the study could play a crucial role in predicting the unit peak discharge at ungauged stations from the known catchment characteristics. Moreover, these findings can also play a crucial role in formulating risk management strategy.

Keywords: catchment, floods, flood characterization, geomorphology, streamflow extremes, unit peak discharge.

47 **1. Introduction**

48 Extremes are, by definition, rare events. These event values would be above (or
49 below) a threshold value close to the upper (or lower) ends of the range of observed values of
50 the variable (Seneviratne et al., 2012). High streamflow extremes (HSE) are of great
51 importance, considering their ability to cause abrupt damage to lives, livelihood,
52 infrastructure, and the environment. Besides, previous studies have shown an increasing trend
53 in HSE in many parts of the world, such as North America (Dethier et al., 2020), Northern
54 Australia (Zhang et al., 2016), United Kingdom (Hannaford & Marsh, 2008). Besides, flood
55 risk is expected to increase in the future worldwide (Arnell & Gosling, 2016; Winsemius et
56 al., 2016). Hence, understanding the relationship between HSE and its causative drivers is of
57 utmost importance to reduce their adverse effects (Blöschl et al., 2017; Gudmundsson et al.,
58 2019; Mallakpour & Villarini, 2015).

59 Trends in extreme rainfall might not fully describe the observed patterns in extreme
60 streamflow trends (Huang et al., 2021; Ivancic & Shaw, 2015). Understanding the
61 relationship between catchment characteristics and HSE globally is difficult because it
62 demands reliable and spatially representative time series data as well as data on possible
63 explanatory variables related to meteorology, climatology, geomorphology, and other
64 catchment features. Existing literature confirms that various geomorphological,
65 climatological, and meteorological drivers impact flooding (Ahn & Merwade, 2016; Al-
66 Rawas & Valeo, 2010; Costa, 1987; Gaume et al., 2009; Marchi et al., 2010; Norbiato et al.,
67 2009; Saharia et al., 2017b). For instance from studying a few largest floods over the
68 continental United States, Costa (1987) concludes that the rain duration and intensity, basin
69 physiography, and geology are primary factors in stimulating runoff. While Saharia et al.
70 (2017a) note that the intense monsoon thunderstorms and steep terrain cause the fastest
71 responding events in the arid Southwest United States. Lun et al. (2021) assess the process

72 controls of flood moments across Europe, examining various catchment-scale characteristics
73 such as precipitation, air temperature, soil moisture, evaporation, aridity, and topography. At
74 the same time, Norbiato et al. (2009) observed that soil properties and geology are among the
75 catchment variables driving the spatial variability of the runoff coefficient and that the mean
76 annual precipitation is the primary driver over 14 eastern Italian Alps catchments. However,
77 existing studies focusing on the characterization of catchments and their floods are primarily
78 limited to the basin- or regional scales, or at most to the continental scale (Marchi et al.,
79 2010). Most existing studies have focused on Europe and the North American continents and
80 have only considered limited factors to characterize catchments (Ahn & Merwade, 2016; Lun
81 et al., 2021; Marchi et al., 2010; Stein et al., 2021).

82 Due to the diversity in catchments worldwide, unraveling the catchment characteristics
83 associated with extreme floods is lacking on a global scale. The existing global databases are
84 sporadic and require significant processing to use together, that could be useful for large-
85 sample and -scale studies. Consequently, it limits our understanding on different factors that
86 influence the HSE globally. Large-scale studies are required to identify the most robust
87 insights on catchment behavior and derive general hydrological principles that can be widely
88 accepted (Addor et al., 2020; Gupta et al., 2014). The importance of large sample studies has
89 been further identified as the foundation of a new paradigm of hydrology, which will
90 contribute toward formulation of new relationships that are hindered by the conventional
91 studies of hydrologic phenomena (Peters-Lidard et al., 2017). A few large-sample and global-
92 scale studies have focused on specific aspects of floods, such as trends and timing (Do et al.,
93 2017; Do, Westra et al., 2020; Gudmundsson et al., 2019; Wasko et al., 2020). But none of
94 them examine how catchment characteristics influence HSE and are limited in terms of the
95 number of geophysical and hydrometeorological explanatory variables that have been
96 included. Moreover, these existing studies usually include catchments with human alterations

97 or anthropogenically-influenced, although anthropogenic alterations significantly impact
98 hydrologic behavior. Thus, there is a need to characterize the least altered catchments at a
99 global scale by utilizing large-sample datasets and a large set of explanatory variables.
100 However, truly pristine catchments are globally sporadic (Hodgkins et al., 2017).

101 This study takes advantage of advanced computational power and multiple global
102 datasets to lay a foundation for developing a comprehensive understanding of HSE globally
103 and advancing our knowledge in the same area. A robust analysis was performed for finding
104 holistic behavior by utilizing a large number of explanatory variables and by examining
105 relationships between HSE and watershed characteristics. Our understanding of the dominant
106 catchment characteristics of HSE from the existing literature is currently limited. Hence, we
107 also tried to assess the relative importance of multiple catchment characteristics with HSE. In
108 this study, a large sample of 45,932 HSE events in 9,710 catchments spread across the globe
109 is used to characterize HSE in catchments with different characteristics employing a large
110 number of explanatory variables.

111 **2. Data Used and Methods**

112 **2.1. Data**

113 Three unique global archives were used to compute and collate hydrological variables
114 of interest and a large number of climatological and geomorphological variables. Extensive
115 pre-processing was performed to match these datasets. Firstly, the annual peak discharge
116 streamflow index, which describes the maximum daily streamflow value in a year, and a
117 small number of catchment characteristics associated with gauge stations spread across the
118 globe were retrieved from the Global Streamflow Indices and Metadata (GSIM) archive (Do
119 et al., 2018; Gudmundsson et al., 2018). Few studies focusing on flood trends and timings
120 have used this variable from the same dataset (Do, Westra, et al., 2020; Wasko et al., 2020).

121 Annual peak discharge is widely used as an indicator of a flood as it allows a straightforward
122 interpretation (Do, Zhao, et al., 2020; Hall et al., 2015; Stein et al., 2020). Since HSE are the
123 rarest events that belong to the upper tail of the observed values, for each station, only the top
124 10 percentile annual peak discharges over the entire time series of observations are
125 considered as HSE events. As it is expected that channels in larger catchments will collect
126 and carry larger discharges, in this study, the HSE values are normalized based on their
127 corresponding drainage area resulting in scale-independent comparisons across catchments.
128 This normalized value called unit peak discharge (UPD) is an important index for studying
129 floods in catchments with different characteristics. For instance, O'Connor & Costa (2004)
130 discussed how catchments producing high unit peak discharge are distributed spatially in the
131 United States and Puerto Rico, and related this index with specific topographic and
132 climatologic conditions. Gaume et al. (2009), Marchi et al. (2010), and Saharia et al. (2017a)
133 utilized this index in envelope curves to characterize floods in Europe and the continental
134 United States, respectively. These curves establish an upper bound for the floods that may be
135 seen in a particular area. Apart from these studies, Lun et al. (2021) have recently
136 investigated the process controls on spatial patterns of flood moments, including the specific
137 mean annual flood, i.e., the mean of unit peak discharge, across European catchments.

138 In order to increase the representation of basin geomorphology, a larger set of
139 variables describing basin characteristics were extracted from the Global Distributed Basin
140 Characteristics (GDBC) database with a spatial resolution of 1 km (Shen et al., 2016). The
141 primary products available in the database include basic characteristics such as basin length,
142 basin area, stream order, stream length, etc. A secondary set of geomorphological variables
143 were derived using the primary products available in GDBC, which includes the elongation
144 ratio that describes basin shape, the bifurcation ratio that is considered a useful measure of
145 proneness to flooding (Allaby, 2008), the relief ratio that measures the overall steepness of

146 drainage basin (Schumm, 1956). They allow for investigation of how the size, shape,
147 structure, and other characteristics might impact floods. Lastly, catchment-averaged
148 meteorological and climatic variables were computed from the 1-km resolution WorldClim
149 datasets (Fick & Hijmans, 2017). The WorldClim datasets variables are derived from the
150 monthly rainfall and temperature averages for the years 1970-2000. The GSIM archive
151 contains streamflow indices of about 30,959 gauge stations. Finally, in order to create a high-
152 quality dataset for carefully selected gauging stations, the following criteria were adopted by
153 balancing data availability, geographical location, quality, and compatibility with other
154 datasets:

- 155 • Since 1,263 gauge stations of GSIM are falling outside the spatial extent of other
156 datasets such as GDBC, these stations were removed from further analysis;
- 157 • To ensure the compatibility between the three sources of datasets, the consistency of
158 geographic coordinates of the GSIM gauge stations was tested. It was observed that
159 most gauge stations do not fall exactly on the streamline concerning the GDBC data.
160 An algorithm was developed to derive compatible coordinates among various
161 datasets. 1) The algorithm uses the drainage area specified in the GSIM for every
162 gauge station and performs a nearest neighbor search based on the corresponding
163 GSIM-provided coordinates over the drainage area map of GDBC to verify if it falls
164 on a river network or not. 2) If the geographical coordinates are relocated, the new
165 coordinates will be used. Otherwise, the same old coordinates are used for retrieving
166 the GDBC data, and 3) Shapefiles are developed for all the 9000+ catchments to
167 derive the catchment-averaged climatological variables from the WorldClim, curve
168 number, information on the landcover, Koppen-Geiger climate, lithology, soil, and the
169 number of dams in the catchments.

- 170 • Only gauge stations with at least 20 years of data with a minimum of 350 daily values
171 each year were selected to ensure robust data. According to Project team ECA&D &
172 Royal Netherlands Meteorological Institute KNMI (2013), the yearly indices
173 computed with 350 daily values are considered to be more reliable.
- 174 • Only GSIM gauge stations whose variable of interest – annual peak discharge – is
175 passing the homogeneity test were utilized in this study. A gauge time series is
176 selected if at least three out of the four tests (the standard normal homogeneity test,
177 the Buishand range test, the Pettitt test, and the von Neumann ratio test) accept the
178 null hypothesis at 99% level. For more details about the homogeneity test, please refer
179 to Gudmundsson et al. (2018). This step ensures that there is no step-change in the
180 time series of annual peak discharge index through its time period that may be
181 possible due to the change in instrumentation, calibration, or damage of the flow
182 measuring instrument or some other reasons (Gudmundsson et al., 2018). It is
183 extremely important as the time-series data of selected gauge stations is available for
184 at least 20 years and a maximum of 133 years for a station within the period 1883-
185 2015. The number of active gauge stations globally reached a peak in the 1980s with
186 more than 8000 stations and have reduced since then as shown in Figure S1.
- 187 • In order to work with undisturbed basins, an attempt was made to remove those that
188 may experience significant anthropogenic influence on the hydrologic cycle. Only
189 stations with an upstream area lower than 10,000 km² were utilized in this study
190 (Kundzewicz et al., 2005; Svensson et al., 2005). In addition, only those gauge
191 stations whose upstream area is devoid of dams are selected, as these catchments are
192 considered less likely to have been modified. The information on dams is retrieved
193 from the Global Reservoir and Dam (GRanD) database (Lehner et al., 2011).
194 Moreover, catchments that are predominantly covered (i.e., more than 50 percent of

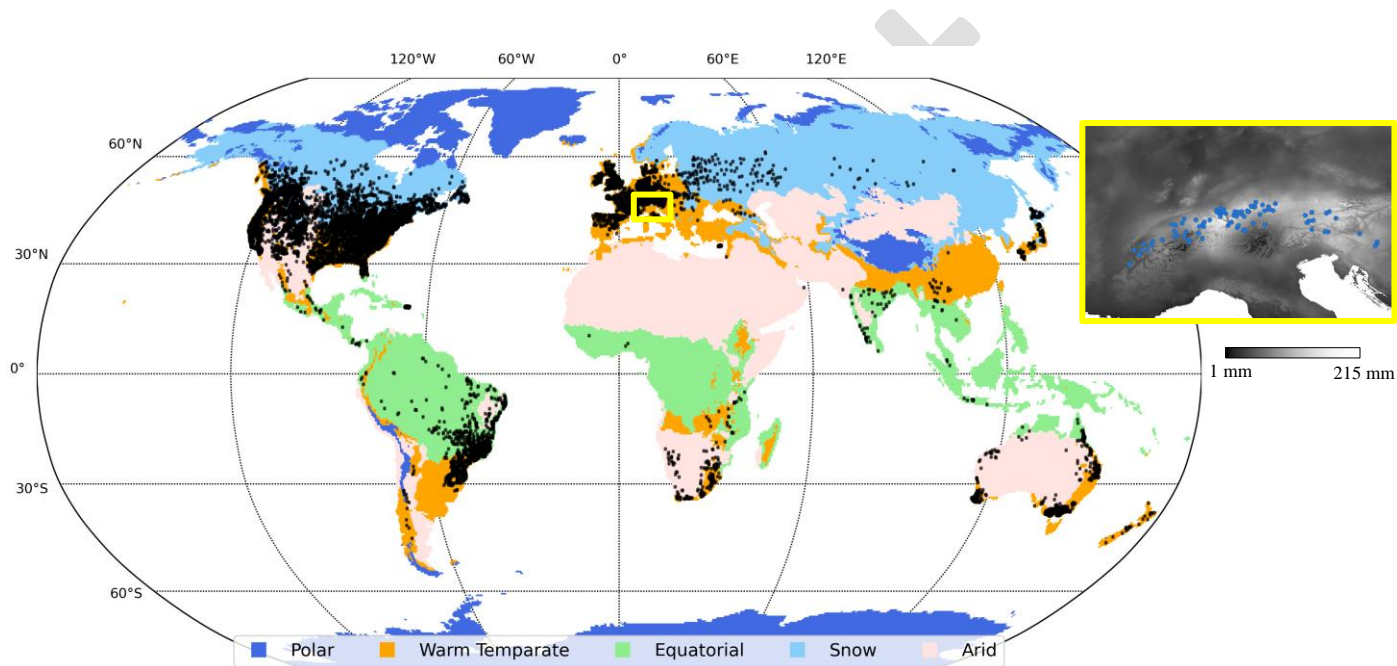
195 its surface area) by the “Settlement” land cover class are also avoided in this study as
196 these catchments would have a considerable anthropogenic influence on its
197 hydrological cycle due to human alterations. This study utilizes the Climate Change
198 Initiative Land Cover (CCI-LC) dataset (<https://maps.elie.ucl.ac.be/CCI/viewer/>)
199 which is available at a spatial resolution of 300 m.

200 After these careful selection criteria, 9,710 gauge stations (catchments) are selected in the
201 final database.

202 **2.2. Study Area**

203 The spatial distribution of the selected gauge stations is shown in Figure 1, overlaid on
204 the Köppen-Geiger main climatic classes (Kottek et al., 2006). The dominant class of a basin
205 is identified as the climate class that spreads over more than 50 percent of the drainage area.
206 The number of catchments in each climatic class is tabulated in Table 1, along with the
207 number of HSE events in total as well as per station. The considerable representation of
208 catchments and HSE events from all the primary climatic classes attests to the robustness of
209 this study. Köppen-Geiger is one of the most widely used climate classification systems. It is
210 an efficient way to aggregate climatic conditions defined by multiple variables and their
211 seasonality with a meaningful classification scheme. Kottek et al. (2006) produced the
212 Köppen-Geiger map based on mean monthly temperature and precipitation data for the period
213 1951 to 2000 from the Climatic Research Unit (CRU) of the University of East Anglia and
214 the Global Precipitation Climatology Centre (GPCC) respectively. The criterion of Köppen-
215 Geiger for the main climates is provided in Table A1 in Appendix. The highest number of
216 catchments are located in the warm temperate climatic class. On the other hand, the lowest
217 number of catchments belong to the polar climatic class. As expected, North America and
218 Europe are densely instrumented compared to other continents. The final dataset is spatially

219 representative across all main climate classes, which will yield unique insights into
 220 hydrologic processes, highlighting the potential of the dataset. The basin averaged values of
 221 geomorphological and climatological information from GDBC and WorldClim, are
 222 augmented to the database to make the comprehensive catchment characteristics database.
 223 The final list of all the explanatory variables from the final dataset, which are being
 224 considered in this study is provided in Table A2 in Appendix.



225
 226 **Figure 1:** The geographic location of all the gauge stations and their associated climatic
 227 classes used in this study. The yellow box projects a cluster of gauge stations whose
 228 catchments are featured with Polar climate, overlaid on a 30-year (1970-2000) average of
 229 August month precipitation.

230
 231 **Table 1:** Number of gauge stations in various climate regions.

Climate region	Number of gauge stations	Number of HSE events	HSE events/Gauge stations
Polar	113	615	5.44
Warm Temperate	4281	19822	4.63
Equatorial	569	2107	3.70
Snow	4075	20459	5.02
Arid	667	2903	4.35
No dominant class	5	26	5.2

233 2.3. Methods

234 The study encompasses the following analyses, detailed in the subsequent sections:

- 235 1. Section 3 reports the spatial distribution of UPD for the highest streamflow extreme
236 events across the globe. Furthermore, to explore the ranges of UPD over different
237 climatic regimes, box plots are employed. Besides, Section 3 summarizes the
238 temporal patterns of all the HSE events over different climates in the northern and
239 southern hemispheres.
- 240 2. Section 4 links the UPD of HSE events to various geomorphological characteristics of
241 catchments, meteorological and climatological variables in Section 5, and to
242 landcover, soil, and lithology in Section 6. These sections explore the first-order
243 dependencies between HSE events and various characteristics of catchments and the
244 variability in these relationships. Firstly, the spearman correlation is computed
245 between the unit peak discharge of all the HSE events and various explanatory
246 variables in the database to evaluate the monotonic relationship between the two
247 variables. Later, box plots for a few highly correlated geomorphological and
248 climatological variables are inspected. In addition, the boxplots for different
249 landcover, lithology, and soils are also investigated for a quick summary of how these
250 land features can influence the UPD of HSE events. Moreover, envelope curves were
251 employed to describe the relationship between drainage area and unit peak discharge.
252 Envelope curves represent the upper limit or envelope of a given data and were used
253 in hydrology studies to provide graphical summaries of extreme floods in various
254 geographical locations across the world (Castellarin, 2007; Crippen & Bue, 1977;
255 Gaume et al., 2009; Kadoya, 1992; Linsley et al., 1949; Saharia, Kirstetter, Vergara,
256 Gourley, & Hong, 2017). A simple power-law formula (Eq.1) is used to plot the
257 envelope curves on log-log graphs:

$$Q = \alpha A^\beta \quad (1)$$

Here $Q(m^3s^{-1}km^{-2})$ is the UPD, $A(km^2)$ is the contributing drainage area, α is the reduced discharge in $(m^3s^{-1}km^{-2(1+\beta)})$, and β is the scaling coefficient. The reduced discharge can be considered an indicator of the magnitude of streamflow by limiting the dependence of the drainage area on the analysis. The β value can be computed by fitting a regression line between $\log(Q)$ and $\log(A)$, as suggested by Castellarin (2007). The β value reflects the change rate of unit peak discharge with the change in the drainage area. The lower the deviation of β value from zero, the lower the unit peak discharge change with the drainage area.

3. Section 7 dictates the relative importance of different catchment characteristics on the target variable – here, unit peak discharge of HSE. For this purpose, a random forest machine learning model is trained with 75% of the events, and its predictions on the remaining 25% of events are evaluated and interpreted using SHAP (Shapley Additive exPlanations) (S. Lundberg & Lee, 2017). Random forests was introduced by Breiman (2001). It features reduced risk of overfitting, ability to interpret, capability to find nonlinear relationships based on multiple predictors that are beyond our capability, good performance, and reliable uncertainty estimates makes it advantageous for successful usage of this approach in our study. Subsequently, the random forest model has shown favorable performance in the past hydrological signature predictions (Addor et al., 2018; Booker & Woods, 2014; Stein et al., 2021). Though direct feature importance methods are popular to highlight the most important variables in the model, SHAP interpretation has the added advantage of explaining how each feature influence alongside which features influence the model providing in-depth model analysis. Moreover, the conventional feature importance methods are not suitable for datasets with correlated features such as the one developed for this

283 study (Degenhardt et al., 2019; Dormann et al., 2013). SHAP not only overcomes the
284 problem of multicollinearity but also considers potential synergistic interactions
285 between variables (S. M. Lundberg et al., 2020). These features of SHAP make it a
286 powerful interpreter and have recently led to successful application in many fields,
287 including water quality assessment (F. Wang et al., 2021; S. Wang et al., 2022).

288 The SHAP summary plot combines feature importance with feature effects. Each
289 point on the summary plot is a Shapley value for a feature and an instance. The
290 Shapley value is the (weighted) average marginal contribution of a feature value
291 across all possible coalitions (Shapley, 1953). The mean absolute value of shapley
292 values over different instances for the given feature gives the overall importance of
293 the corresponding feature on the target variable - UPD. Overall, the SHAP summary
294 plot demonstrates:

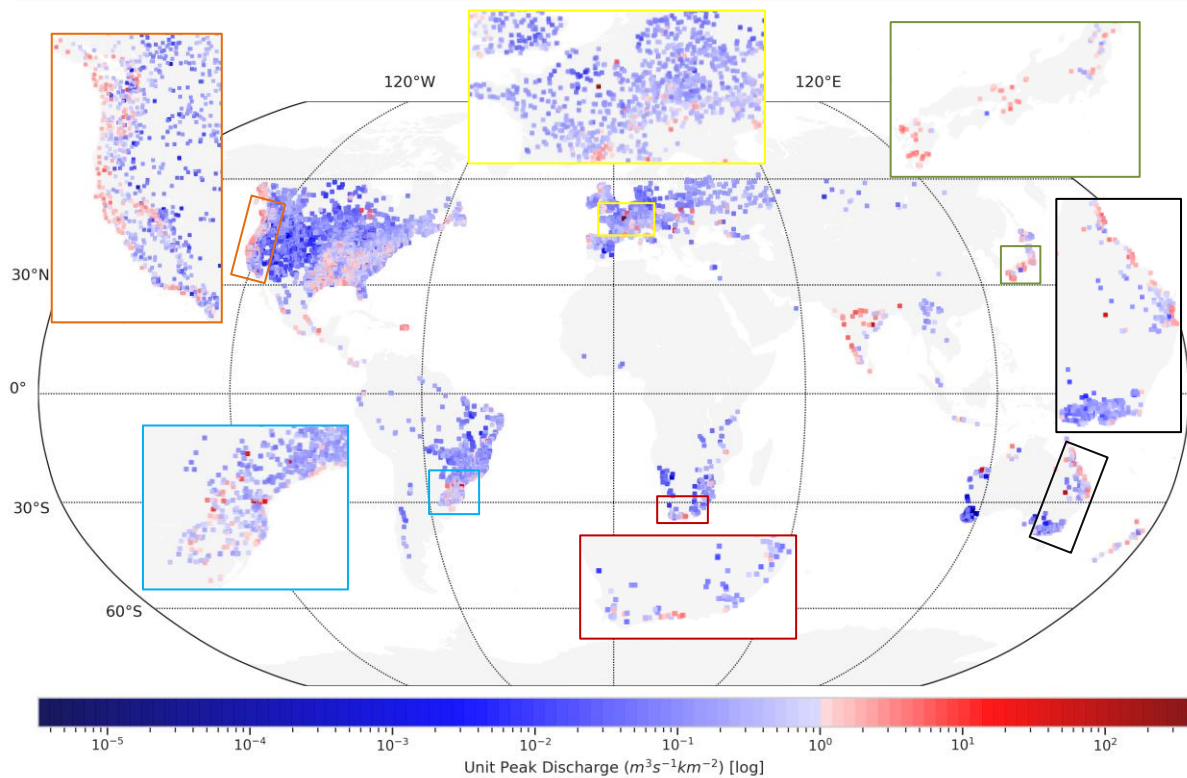
- 295 • Feature importance – the order of the features along the y-axis is based on
296 their importance in descending order. The higher (lesser) the absolute mean
297 value of SHAP values provided on the right side of the features name in the
298 plot, the higher (lesser) its relative importance.
- 299 • Impact – the horizontal location of the dots depicts the intensity of its
300 influence on predictions. Zero values on the x-axis indicate no impact, and
301 positive (negative) values towards the rights (left) side indicate positive
302 (negative) impact.
- 303 • Original value- the color of the dots represents the values of the corresponding
304 features if it is high (red) or low (blue) for that observation in the dataset.
- 305 • Correlation- the combined observations of the distribution of dots along the x-
306 axis and their color describe the correlation of the features with the target
307 variable.

308 3. Spatial and temporal distribution of the HSE events across the globe

309 Unit peak discharge provides the advantage of allowing the comparison of flooding
310 characteristics across a wide variety of spatial scales. Figure 2 presents the spatial distribution
311 of UPD of the highest streamflow extreme event recorded over the respective gauge stations
312 across the globe from the database. Similar to the floods in continental United States and
313 Europe that were examined by Saharia et al. (2017a), Marchi et al. (2010), and Gaume et al.
314 (2009), it is observed that the highest UPDs occur over mountainous terrain along oceans, as
315 exemplified by the Cevennes-Vivarais Mediterranean region in France, the West Coast of the
316 continental United States, the coast of western provinces of British Columbia and Yukon in
317 Canada, the west coast of the Canadian island of Newfoundland, the Hidalgo region of
318 Mexico, the northeast region of the Great Dividing Range in Australia, windward side of
319 Cape fold mountains range in South Africa and India's Western Ghats region. In contrast, the
320 unit peak discharge is comparatively low on the leeward side along the Andes Mountains
321 range nearer to the South Pacific Ocean, the leeward side of the Australian Alps in Australia,
322 and the leeward side of the Drakensberg Mountain range in Africa, as expected. Moreover,
323 from the preliminary observations of the database and spatial patterns in Figure 2, it is
324 observed that many catchments in North and South America having high UPD values belong
325 to the Warm Temperate climate type and are predominantly covered by agriculture and forest
326 landcover. Argentina witnesses some of the most intense mesoscale convective systems on
327 Earth. A field campaign known as RELAMPAGO-CACTI highlighted how deep convection
328 frequently initiates in this region, especially along the complex terrain of Sierras de Córdoba
329 and Andes, and often grows rapidly upscale into dangerous storms resulting in intense flash
330 flooding (Pal et al., 2021). Besides, the geomorphologic characteristics of large parts of its
331 territory make Argentina highly vulnerable to floods. For instance, many of the fluvial
332 systems of the country are connected to mountain environments, such as the Pampean and

333 Cordillera Ranges, along with the Sub-Andean and Eastern Cordillera Ranges, which receive
334 intense and concentrated rainfall during the summertime leading to flash floods in these
335 rivers (Latrubesse & Brea, 2009). Interestingly, most of the European catchments with high
336 UPDs are also dominantly covered by forest or agricultural landcover. Importantly, most of
337 these catchments are of small size. Marchi et al. (2010) reported that a few of the most
338 extreme flash floods and their characteristics across Europe are attributed to small catchment
339 areas. Besides, Brebbia & Katsifarakis, (2007) note that the geo-hydrological conditions of
340 heavy rainfall combined with steep slopes and deep valleys in small Mediterranean
341 catchments produce higher UPD. The possible reasons for high UPDs in forest and
342 agriculture dominated catchments is explained in detail in Section 6.

343 At the same time, Indian catchments display among the highest UPDs and belong to
344 the Equatorial climatic class. They receive very high rainfall due to synoptic scale monsoon
345 disturbances during July and August, with 80 percent of the annual rainfall occurring during
346 the southwest monsoon rainfall from June to September. Besides, these catchments are also
347 mostly covered by agricultural and forest. Detailed reasoning for these characteristics is
348 explained in subsequent sections. In comparison, the lowest unit peak discharge producing
349 catchments were recorded in Australia. Most of them belong to the warm temperate climatic
350 class and are dominated by unconsolidated sedimentary type lithology within their catchment
351 boundaries. Detailed reasoning for these landcover and geologic characteristics is explained
352 in Section 6. There is a diversity of factors that may cause high and low unit peak discharges
353 that need to be explored. Detailed analyses and explanatory attributions are provided in the
354 subsequent sections.

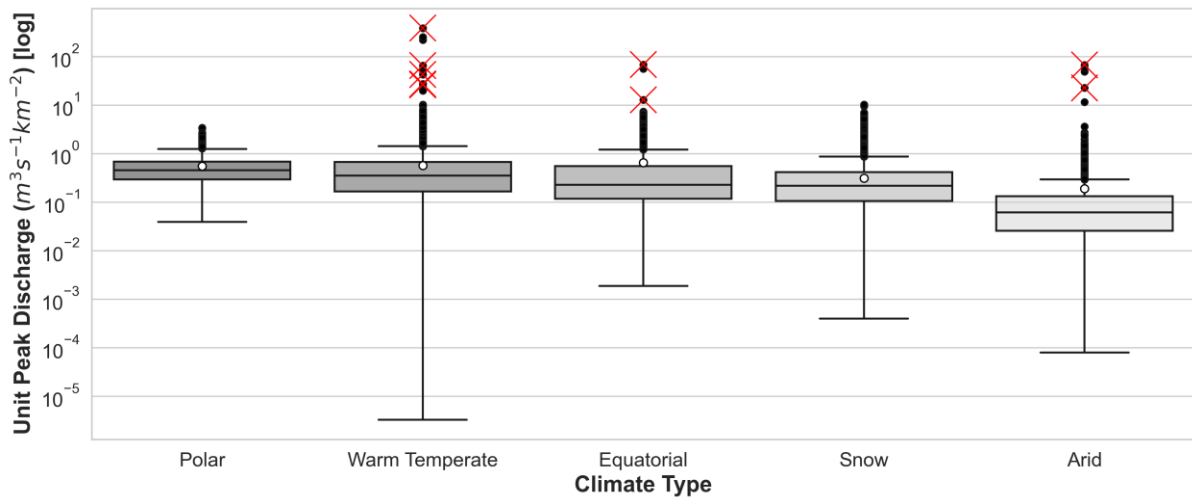


355

356 **Figure 2:** Spatial distribution of unit peak discharge for the highest streamflow events
 357 recorded over the corresponding gauge stations across the globe.

358 A wide variety of variables dictate the spatial differences in the magnitude of unit
 359 peak discharge across the globe. To explore the dependence of HSE on climatic regimes, the
 360 five main climatic classes (Table 1) were utilized in this study - Polar, Warm Temperate,
 361 Equatorial, Snow, and Arid. To get a quick summary of the ranges of UPDs of all the HSE
 362 events in different climatic classes, Figure 3 displays box and whisker plots for different
 363 climatic classes. The top ten catchments in terms of high UPD values are highlighted with red
 364 color cross marks. Seven out of ten high UPDs belong to catchments with Warm Temperate
 365 climate. Moreover, the mean of all the HSE events in this group is higher than any other
 366 climate type. At the same time, the median of UPDs in the Polar climatic class is maximum.
 367 In contrast, both the mean and median of UPD are low in the case of HSE events over Arid
 368 regions. The high mean and median of the Polar class could be an artifact of the small sample
 369 of catchments (113) compared to the other climate classes (Table 1), with most of them (92)
 370 clustered in the central part of Europe spread over Switzerland, Austria, Germany, and
 371 France, which are highlighted with a yellow box in Figure 1. This region experiences high

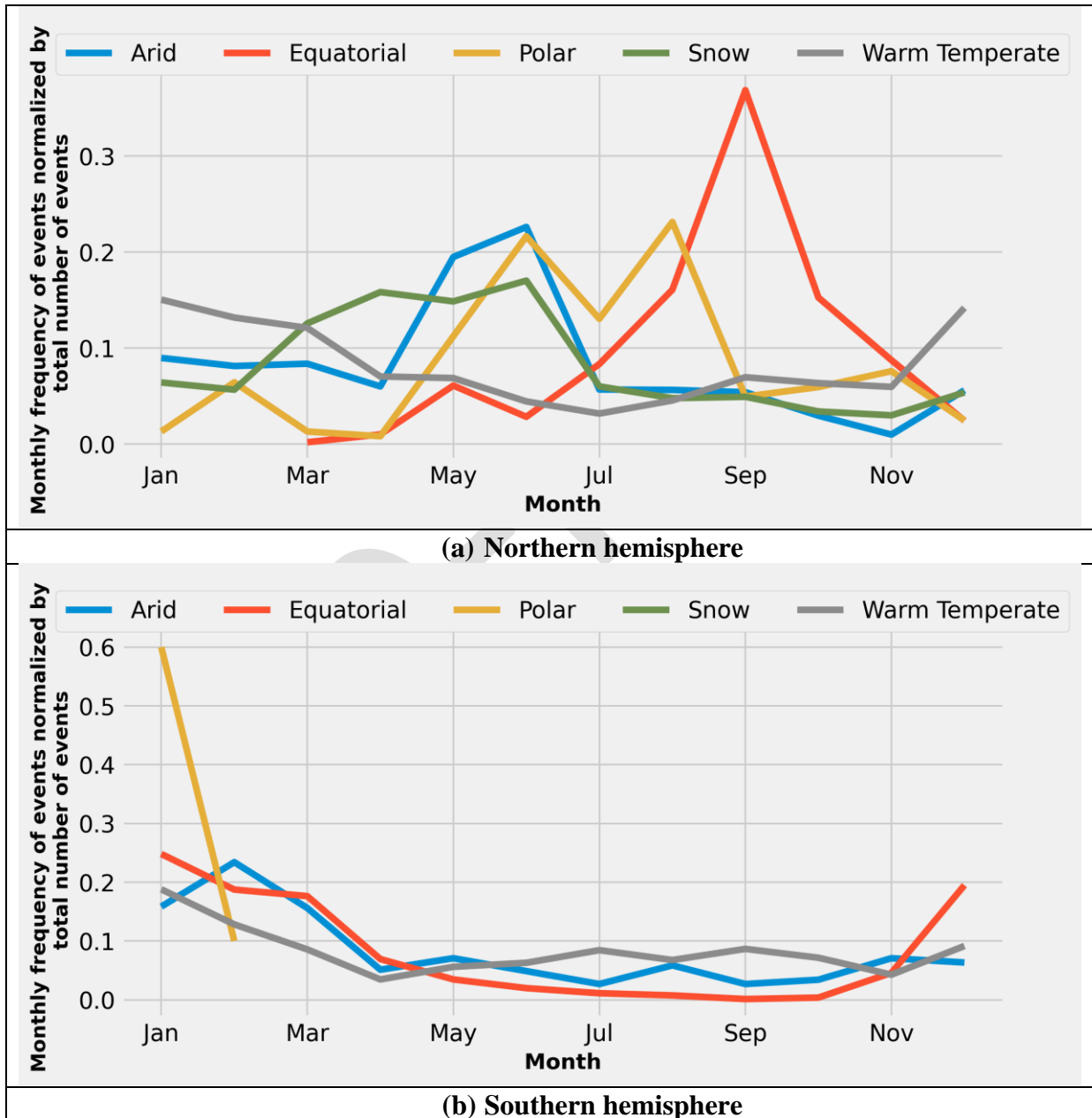
372 precipitation from June to August, as shown in Figure 1. Subsequently, the frequency of HSE
 373 events in the Polar climate dominant catchments in the northern hemisphere is high from June
 374 to August, as shown in Figure 4(a). Besides, almost half (57) of the sample of Polar
 375 catchments are identified to have forest landcover type, and majority of them dominantly
 376 have cambisols type soil (79) and sedimentary type lithology broadly (83).



377 **Figure 3:** Box-and-Whisker plot of unit peak discharge for different climatic classes. The
 378 box spans the interquartile range in the plot, i.e., the upper and lower ends of the box
 379 correspond to the first quartile and third quartiles, respectively. The whiskers are the two
 380 vertical lines outside the box extended until the observations' extremes. The median is
 381 marked by a horizontal line inside the box, and the mean is plotted with a white circle. The
 382 black circles beyond the extremes are considered outliers at a distance of more than 1.5 times
 383 the interquartile range. The red cross marks correspond to the top ten catchments in terms of
 384 high unit peak discharge values.
 385

386 Figure 4 shows the temporal distribution of the HSE events over different months
 387 normalized by the total number of events in different climatic classes. Since there will be a
 388 difference in seasons between the northern hemisphere (NH) and the southern hemisphere
 389 (SH) by almost 6 months, separate temporal distribution plots have been plotted for these two
 390 regions (Figure 4(a) and 4(b)) resulting in rational plots on the temporal patterns of HSE
 391 events in different seasons and climatic classes. It is observed that most of the HSE events in
 392 the catchments dominated by Polar climate are observed in summer in both NH and SH.
 393 Whereas in Arid climate catchments, most of the HSE events over NH and SH are caused in
 394 May and June, and January to March, respectively. Similarly, Snow climate catchments in the

395 NH experience most HSE events between April and June. In contrast, most of the HSE events
 396 in the catchments dominated by warm temperate climates are observed between December
 397 and February at NH and SH. At the same time, over Equatorial catchments in NH and SH,
 398 these extreme events are observed maximum from August to October and December to
 399 March, respectively.



400

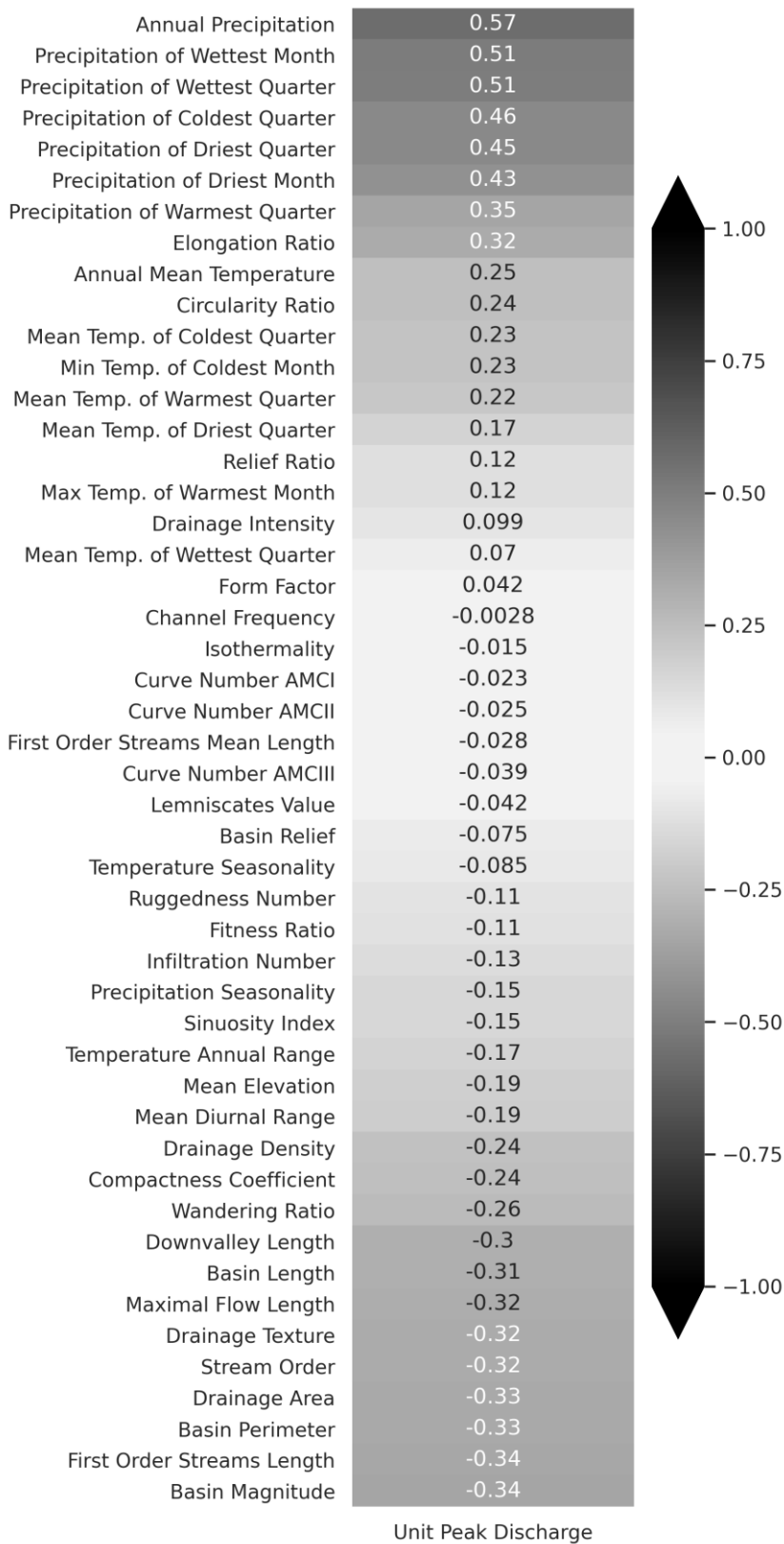
401 **Figure 4:** Monthly distribution of high streamflow extreme (HSE) events normalized by the
 402 total number of events in different climate classes.

403 **4. Exploring the first-order relationship between HSE events and various**
404 **geomorphological characteristics of catchments**

405 Figure 5 displays the spearman-correlation coefficient values between the UPD and
406 the geomorphological, meteorological, and climatological variables. It is noteworthy that the
407 meteorological variables display a higher correlation among other variables.

408 Figure 5 reveals that geomorphological catchment characteristics such as the basin
409 magnitude, first-order streams length, basin perimeter, drainage area, stream order, and
410 elongation ratio are highly correlated with the unit peak discharge. In addition, maximal flow
411 length, drainage texture, and basin length also have higher correlation among the remaining
412 geomorphological characteristics. Among the above-mentioned list of variables, except for
413 the elongation ratio of the catchment, all are negatively correlated with the unit peak
414 discharge. In contrast, the elongation ratio is positively correlated. Basin magnitude is the
415 total number of first-order streams within the catchment boundary (Costa, 1987). In
416 comparison, the first-order streams length is the sum of all these first-order streams in a
417 catchment boundary. The first-order streams are known to be the outermost tributaries, and
418 the overland flow of water dominates them (O'Briain, 2020). In addition, these streams flow
419 into and feed the higher-order streams. As the length of the first-order streams increases, the
420 streamflow takes more time to reach the higher-order streams/outlet and leads to lower UPD.
421 The drainage area indicates the total geographical area contributing to the flow accumulation
422 corresponding to its outlet location. In general, outlets of higher-order streams will have
423 higher contributing drainage areas, which leads to higher streamflow travel time that results
424 in lower unit peak discharges. Moreover, the basin perimeter, maximal flow length, and basin
425 length increase with drainage area and stream order. Hence, an increase in these variables
426 will lead to lower unit peak discharges. Here maximal flow length corresponds to the length
427 along the most extended stream from the head of the channel to the outlet. Simultaneously,

428 basin length corresponds to the most extended length of the line from a basin outlet to a point
429 on the perimeter equidistant from the basin outlet in either direction around the perimeter
430 (Gregory & Walling, 1968). According to Schumm (1956), the elongation ratio is the ratio
431 between the diameter of a circle of the same area as the catchment and the maximum length
432 of the catchment. This ratio describes the shape of the catchment. Higher ratios indicate that
433 the corresponding catchment is circular, and the lower elongation ratio indicates that the
434 catchment shape is elongated. Circular catchments with a higher elongation ratio are more
435 efficient in runoff routing, and flow accumulates in less time in such catchments
436 (Subramanya, 1984). Hence, an increase in the elongation ratio may increase the unit peak
437 discharge. The boxplots of basin magnitude (Figure S3(a)) and drainage area (Figure S3(b))
438 for different climatic classes and their explanation are available in supplementary file. It
439 depicts how those two relatively highly correlated geomorphological variables vary among
440 different climate regions.



441

442

443

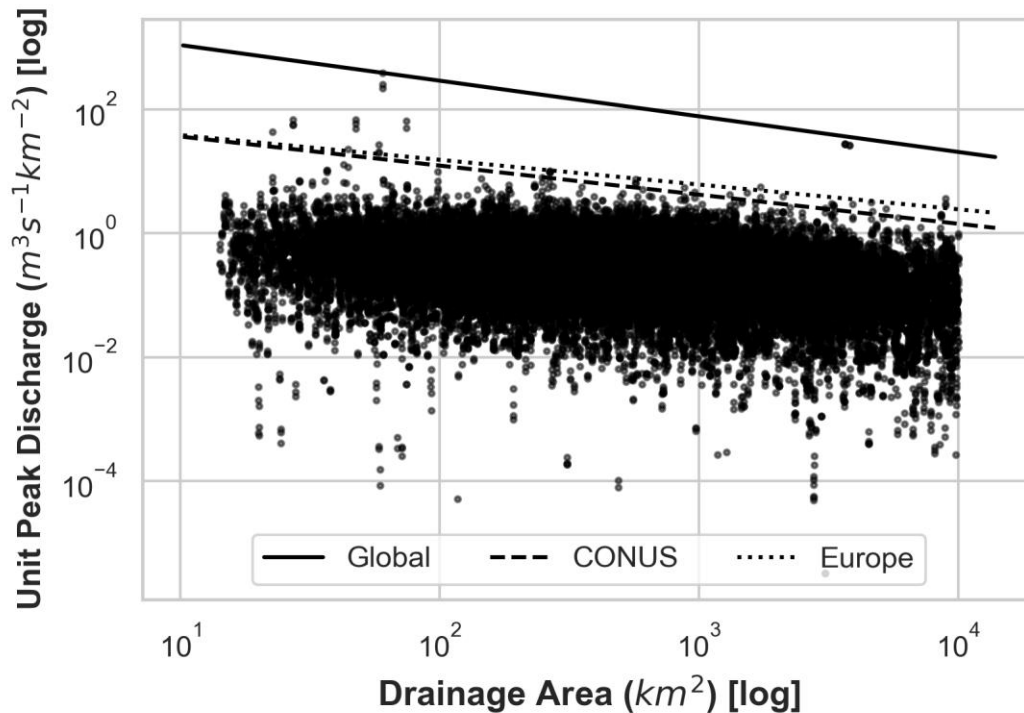
444

Figure 5: Spearman-correlation coefficients between unit peak discharge of all the high streamflow events and multiple catchment characteristics. The values range from 1 to -1. The positive values represent a positive correlation, with 1 being the highest/perfect positive

445 correlation, while the negative values represent a negative correlation, with -1 being the
446 highest/perfect negative correlation. A value equal to 0 represents no correlation.

447

448 The upper envelope curve for the whole sample is shown in Figure 6 as a solid line.
449 The envelope curves of extreme floods in the continental US and Europe that are reported in
450 existing literature are also plotted for comparison (Gaume et al., 2009; Saharia et al., 2017a).
451 The α and β values of the envelope curve for the global sample were estimated to be 4130.60
452 and -0.58. Saharia et al. (2017a) reported the α and β values for the continental United States
453 region to be 108 and -0.47. Similar values of 97.0 and -0.40 were reported for Europe by
454 Gaume et al. (2009). Since the deviation of β value from zero is more in the case of an
455 envelope curve for HSE across the globe, the rate of change of unit peak discharge with the
456 change in the drainage area is faster than continental United States and Europe catchments.
457 Moreover, the higher α value of the global sample, when compared with values reported for
458 the continental United States and Europe, indicates that the maximum magnitude of floods
459 across the globe is much higher than those reported in their respective continents.



460

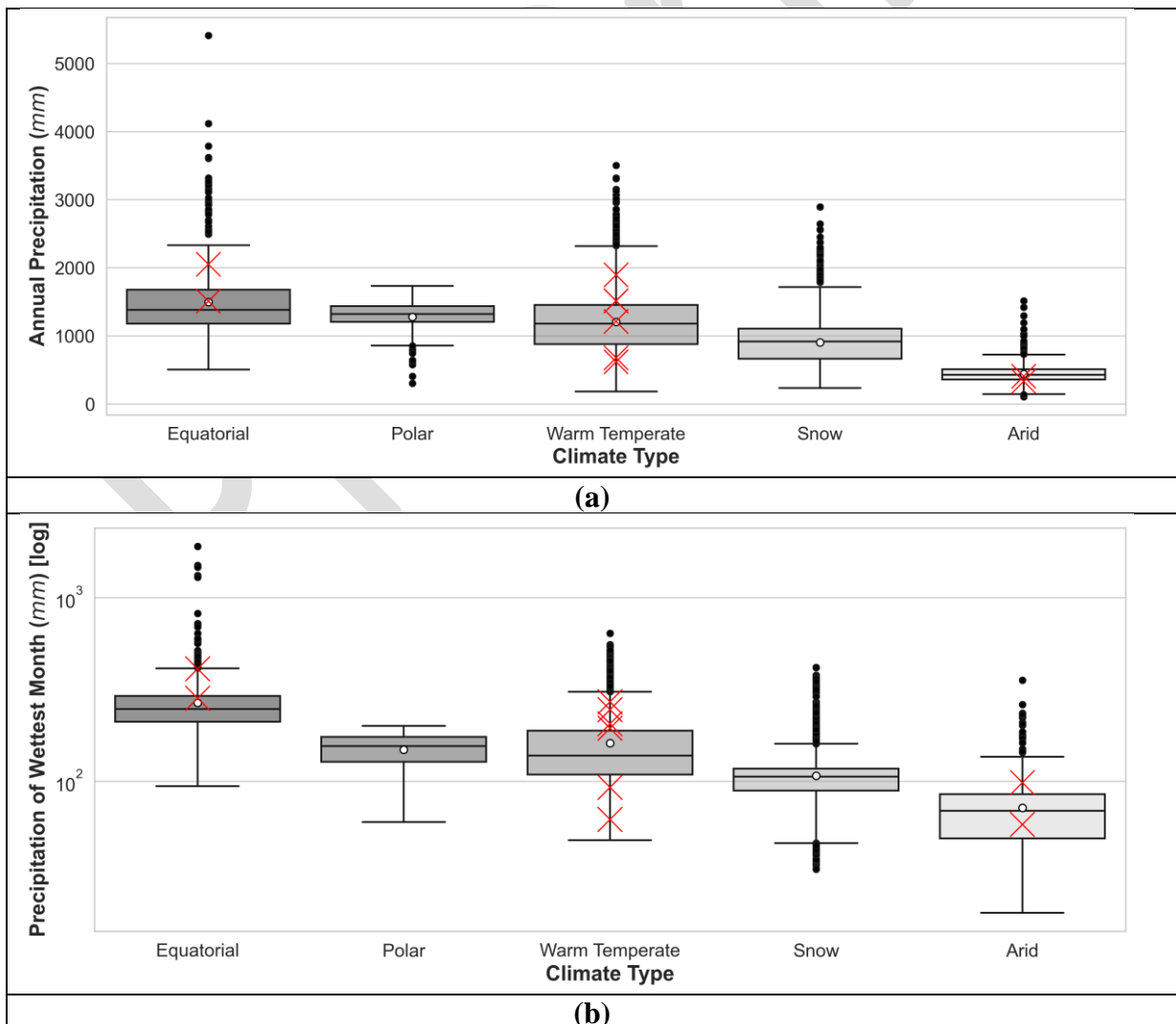
461 **Figure 6:** Unit peak discharge vs. drainage area along with their envelope curves for all the
 462 high streamflow extreme (HSE) events across the globe. The envelope curves for continental
 463 United States and Europe are taken from Marchi et al. (2010) and Saharia et al. (2017a).

464

465 5. Exploring the first-order relationship between HSE events and various 466 meteorological and climatological characteristics of catchments

467 To explore the meteorological and climatological catchment characteristics that
 468 influence HSE, the correlation between relevant variables and the magnitude of unit peak
 469 discharge is studied first. From Figure 5, the annual precipitation has the highest correlation
 470 among all the explanatory variables available in the database, followed by precipitation of the
 471 wettest month, precipitation of wettest quarter, precipitation of coldest quarter, among other
 472 meteorological indices. As expected, all these variables are positively correlated with the unit
 473 peak discharge. Meteorological factors are considered to be the primary driver for streamflow
 474 generation across most climates (Berghuijs et al., 2019; Norbiato et al., 2009; O'Connor &
 475 Costa, 2004; Saharia et al., 2017a). The boxplot of annual precipitation for different climatic

476 classes is plotted in Figure 7(a). It is observed that the maximum precipitation (5413.7 mm) is
 477 recorded in a catchment belonging to the Equatorial climatic class. Equatorial has the highest
 478 mean, median, and quartile values, and it is followed by the Polar climatic class, whereas the
 479 lowest was recorded in the Arid climatic class, followed by the Snow class. Similar
 480 observations are found in the boxplot of precipitation of wettest month for different climatic
 481 classes (Figure 7(b)). These observations explain why the Equatorial catchments can produce
 482 high unit peak discharge, as observed in Figure 3, though the geomorphology of the same
 483 catchments is generally not favorable to produce high annual peak discharge, unlike
 484 catchments in the Polar or the Warm Temperate climatic classes. These insights also further
 485 confirm that the HSE nature is influenced by a multitude of physiographic variables.



486 **Figure 7:** Box-and-Whisker plot of (a) annual precipitation and (b) precipitation of wettest
487 month for different climatic classes. The red cross marks correspond to the top ten
488 catchments in terms of high unit peak discharge values. *Please refer to the caption of Figure*
489 *3 for the description of the box plots.*

490 **6. Exploring the relationship between HSE events and catchment characteristics**

491 Besides the basin characteristics related to geomorphology and climatology, other
492 landscape variables related to soil and land cover play an important role in how precipitation
493 is converted to runoff. In this section, we analyze how land cover, lithology, and soil type
494 within the catchment boundary relate to the UPD of HSE and how it varies in different
495 climates.

496 The dominant land cover within a catchment is expected to play a significant role in
497 the runoff generation process and thus the unit peak discharge, as confirmed by several
498 studies (Ahn & Merwade, 2016; Ashraf M. & Yasushi, 2008; Kiran et al., 2017; Woltemade
499 et al., 2020). The change in land use and land cover alters the geomorphology of the
500 catchment, eventually affecting floods (Cao et al., 2020). Here, we assess the impact of land
501 cover on UPD in different climate zones. In the database, the gauge stations are classified into
502 nine land cover types based on a dominant characteristic (covering more than 50 %
503 catchment area). If any of the catchments do not have a dominant land cover type, they are
504 classified as “No dominant class”. The box-and-whisker plots in Figure S4 confirm that the
505 magnitude of the unit peak discharge varies for different land cover types across all the
506 climates. Catchments with the greater grassland, followed by forest landcover in polar
507 climates display considerably higher mean and median (0.631 and $0.502 \text{ m}^3\text{s}^{-1}\text{km}^{-2}$) values
508 of UPD compared to the bare area ($0.076 \text{ m}^3\text{s}^{-1}\text{km}^{-2}$), respectively. According to the Food
509 and Agriculture Organization (FOA) of the United Nations, bare area corresponds to areas
510 that do not have any artificial cover due to human activities and includes bare rock areas,
511 sands, and deserts. As the sands and deserts have very high infiltration capacity, the median

512 unit peak discharge is low in these areas. Moreover, the lithology type, soil type, and
513 physiographic and meteorological conditions in bare areas would have a substantial impact
514 on the magnitude of runoff generation. The catchments dominated by wetland in warm
515 temperate ($0.625 \text{ m}^3 \text{ s}^{-1} \text{ km}^{-2}$) and arid ($0.137 \text{ m}^3 \text{ s}^{-1} \text{ km}^{-2}$) climates are observed to have
516 high median values in those respective climates relative to other landcover dominated
517 catchments. In contrast, wetland catchments showcase the least median ($0.050 \text{ m}^3 \text{ s}^{-1} \text{ km}^{-2}$)
518 and mean UPD values in snow climates relative to other landcovers in the same climate.
519 Also, permanent ice, followed by bare area and water have higher median values of UPD in
520 snow climates. At the same time, sparse vegetation dominated catchments are observed to
521 have the least median ($0.034 \text{ m}^3 \text{ s}^{-1} \text{ km}^{-2}$) in case of warm temperate climates and have
522 second highest median UPD value ($0.087 \text{ m}^3 \text{ s}^{-1} \text{ km}^{-2}$) among others in case of arid
523 climates, respectively. Subsequently, forest and grassland dominated catchments of
524 Equatorial and warm temperate (immediately after and close to wetland and water) climates
525 have relatively higher UPD values in their respective climate catchments. Overall, the highest
526 median value was recorded in permanent ice landcover with $0.694 \text{ m}^3 \text{ s}^{-1} \text{ km}^{-2}$, followed by
527 catchments that are dominantly covered by grassland with $0.328 \text{ m}^3 \text{ s}^{-1} \text{ km}^{-2}$, and forest
528 with $0.318 \text{ m}^3 \text{ s}^{-1} \text{ km}^{-2}$.

529 Besides, most of the top 10 catchments corresponding to the highest HSE events
530 belong to forest and/or agriculture-dominated catchments across the climates. Agricultural
531 practices, such as tillage, alter soil porosity and soil structure, which results in a reduction of
532 soil infiltration rate and consequently increases surface runoff (Owuor et al., 2016).
533 Moreover, the establishment and extension of roadside culverts, ditches, and irrigation canals
534 in agriculture-dominated areas create new gullies and channel networks (Dijck, 2000). This
535 phenomenon results in high stream frequency and quick overland flow of runoff in
536 agricultural dominated catchments, and in high unit peak discharge.

537 Though lithology has been identified to have an impact on flooding (Gaume & Borga,
538 2008; Norbiato et al., 2009), very few studies have explored how the lithology of a catchment
539 influences its magnitude. Hence the relationship between the unit peak discharge and the
540 lithology type that is dominant (occupying more than 50% of the area, else “No dominant
541 type”) was assessed. Box plots of unit peak discharge for different lithology types over all the
542 main climates are plotted in Figure S5. It is evident that the highest median values in Polar
543 climate catchments are recorded in mixed sedimentary rocks ($0.379 \text{ m}^3 \text{ s}^{-1} \text{ km}^{-2}$), followed
544 by acid volcanic rocks ($0.379 \text{ m}^3 \text{ s}^{-1} \text{ km}^{-2}$), and unconsolidated sediments (0.379
545 $\text{ m}^3 \text{ s}^{-1} \text{ km}^{-2}$). While intermediate volcanic rocks ($0.379 \text{ m}^3 \text{ s}^{-1} \text{ km}^{-2}$), followed by acid
546 plutonic rocks ($0.379 \text{ m}^3 \text{ s}^{-1} \text{ km}^{-2}$), have significantly less median UPD values among others
547 in the polar climates. Sedimentary rocks such as modern claystone and mudstones, composed
548 primarily of clay minerals, have little permeability. It is also noteworthy that the thickness of
549 regolith plays a crucial role in hydrological connectivity between the surface and the
550 subsurface system of a catchment (Bonanno et al., 2021; Gourdol et al., 2021). Besides, as
551 per Miyaoka et al., (1999), in some sedimentary catchments, the regolith layer is thinner than
552 the intrusive igneous catchments. Due to the thinner regolith, runoff generation is much
553 higher in catchments with sedimentary bedrocks than in igneous bedrock catchments when
554 other catchment characteristics are favorable. Precipitation percolates into the fractured
555 bedrock, mixes with soil water in the regolith, and discharges quickly into the sedimentary
556 rock catchment (Miyaoka et al., 1999).

557 At the same time, intermediate volcanic rocks, followed by acid volcanic rocks in the
558 warm temperate climate, have high median UPD values, among others. However, there is
559 little difference in median values among each other, indicating that the lithology type has
560 little influence on HSE in catchments with warm temperate climates.

561 Pyroclastics followed by basic volcanic rocks dominated catchments are observed to
562 have high median values in equatorial climate catchments. While mixed sedimentary and
563 unconsolidated sediments, both in the case of equatorial and warm temperate, have relatively
564 lower median UPD values in their respective climates. In the case of ice and glaciers, basic
565 plutonic rocks are connected to relatively high median values. Whereas intermediate volcanic
566 rocks, followed by acid plutonic rocks and acid volcanic rocks, have high and low median
567 values in arid climates, respectively. Basic plutonic rocks and basic volcanic rocks are
568 igneous rocks that are also known to be primary rocks that have high unit peak discharge.
569 Basic rocks are characterized by less silica content. Basic oxides in the basic rocks make both
570 basic plutonic rocks and volcanic rocks much denser and more compact. Generally, water
571 tends to flow quickly without any infiltration over these types of rocks, which may result in
572 high median unit peak discharges. However, the hydrologic connectivity across complex
573 structure catchments is also influenced by the interaction between soil zone water tables,
574 deeper bedrock aquifers, and the potential spatial variability of these integrations (Jencso &
575 McGlynn, 2011).

576

577 The infiltration capacity, soil moisture holding capacity, and other soil properties
578 corresponding to each soil type will impact the magnitude of streamflow or floods (Ahn &
579 Merwade, 2016; Berghuijs et al., 2019; Ivancic & Shaw, 2015; Kuntla, 2021; Norbiato et al.,
580 2009). Box plots of unit peak discharge for different soil types over all the climates are
581 plotted in Figure S6. Catchments with cambisols have maximum median value in the polar
582 climates ($0.483 \text{ m}^3 \text{ s}^{-1} \text{ km}^{-2}$). Whereas, in the warm temperate climates, high median values
583 of UPD are observed in fluvisols, followed by podsols and nitisols dominated catchments.
584 Nitisols allow water to drain at a moderate rate with a 30 percent clay in its subsurface
585 horizon. These are mostly found in level to hilly land under tropical rain forests or savannah

586 vegetation. While in arid climates, catchments dominated by vertisols possess high median
587 UPD, followed by ferralsols. Likewise, vertisols showcase high median values in Equatorial
588 climates. In contrast, catchments dominated by solonetz soil type had the lowest median
589 value ($0.013 \text{ m}^3\text{s}^{-1}\text{km}^{-2}$). The parent material of solonetz type soil is unconsolidated
590 materials. Moreover, they are associated with a flatlands and steppe climate including dry
591 summers and annual precipitation of less than 400-500 mm (Land and Water Division, 2006).
592 Hence, catchments dominated by this soil type may have lower median unit peak discharge.
593 Gleysols, followed by alisols dominated catchments are observed to have high median UPD
594 values in the Snow climate. At the same time, most of the top 10 severe floods across all the
595 climates observed to be associated with ferralsols and/or cambisols (see Figure 8(c)).
596 Ferralsols represent the classical soils weathered from basic rocks. These are exclusively
597 found in Africa and South America in humid tropics and in regions in southeast Asia where
598 the climate is hot and humid with easily weathering basic rocks (Land and Water Division,
599 2006). They are well-drained but have low water storage capacity. Due to their geographic
600 locations, climate, and meteorological conditions and properties, out of the ten highest unit
601 peak discharges, most are associated with basins recorded here.

602 Further comprehensive reasoning and investigation into the influence of landcover,
603 lithology, and soil types on UPD or floods, in general, is beyond the scope of this study.

604 **7. Relative Importance of catchment characteristics on HSE**

605 As it is observed that extreme events share a complex nonlinear relationship and are a result
606 of an interplay between a multitude of catchment variables in the earlier sections, here in this
607 section, we perform a multidimensional analysis of catchment characteristics on HSE
608 utilizing a random forest model and SHAP. The multidimensional analysis in this section is
609 also carried out based on main climates wise, resulting in detailed insights on dominant

610 variables in each climatic class. The accuracy statistics of the model predictions for the
 611 remaining 25% of the events, compared with their corresponding observation values for
 612 different climatic classes, are tabulated in Table 2.

613 **Table 2:** Random Forest model predictions statistics

Climate region	Statistic	Value
Polar	Accuracy	84.9 %
	Mean absolute error	0.08
Warm Temperate	Accuracy	68.37 %
	Mean absolute error	0.14
Equatorial	Accuracy	83.84 %
	Mean absolute error	0.11
Snow	Accuracy	80.88 %
	Mean absolute error	0.06
Arid	Accuracy	67.81 %
	Mean absolute error	0.04

614
 615 Annual precipitation, precipitation of driest month, precipitation of wettest quarter, min.
 616 temperature of coldest month and ruggedness number are observed to be the top 5 influencing
 617 features in the polar climate dominant catchments according to the SHAP summary plot
 618 (Figure 8(a)). In addition, it confirms that annual precipitation and precipitation of driest
 619 month and wettest quarter are positively correlated, as seen in the first-order analysis of this
 620 study, with a capacity of influencing the SHAP value of UPD by ± 0.1 alone. Also, the lower
 621 values of the minimum temperature of coldest month have a negative impact on modeling
 622 UPD with more intensity compared to the positive impact of the higher values. At the same
 623 time, lower ruggedness number values have a high-intensity positive impact on the model
 624 compared to the negative impact of the higher values.

625 In the case of warm temperate dominated catchments, as per Figure 8(b), and the mean
 626 absolute value of the SHAP values, precipitation of wettest month, precipitation of wettest

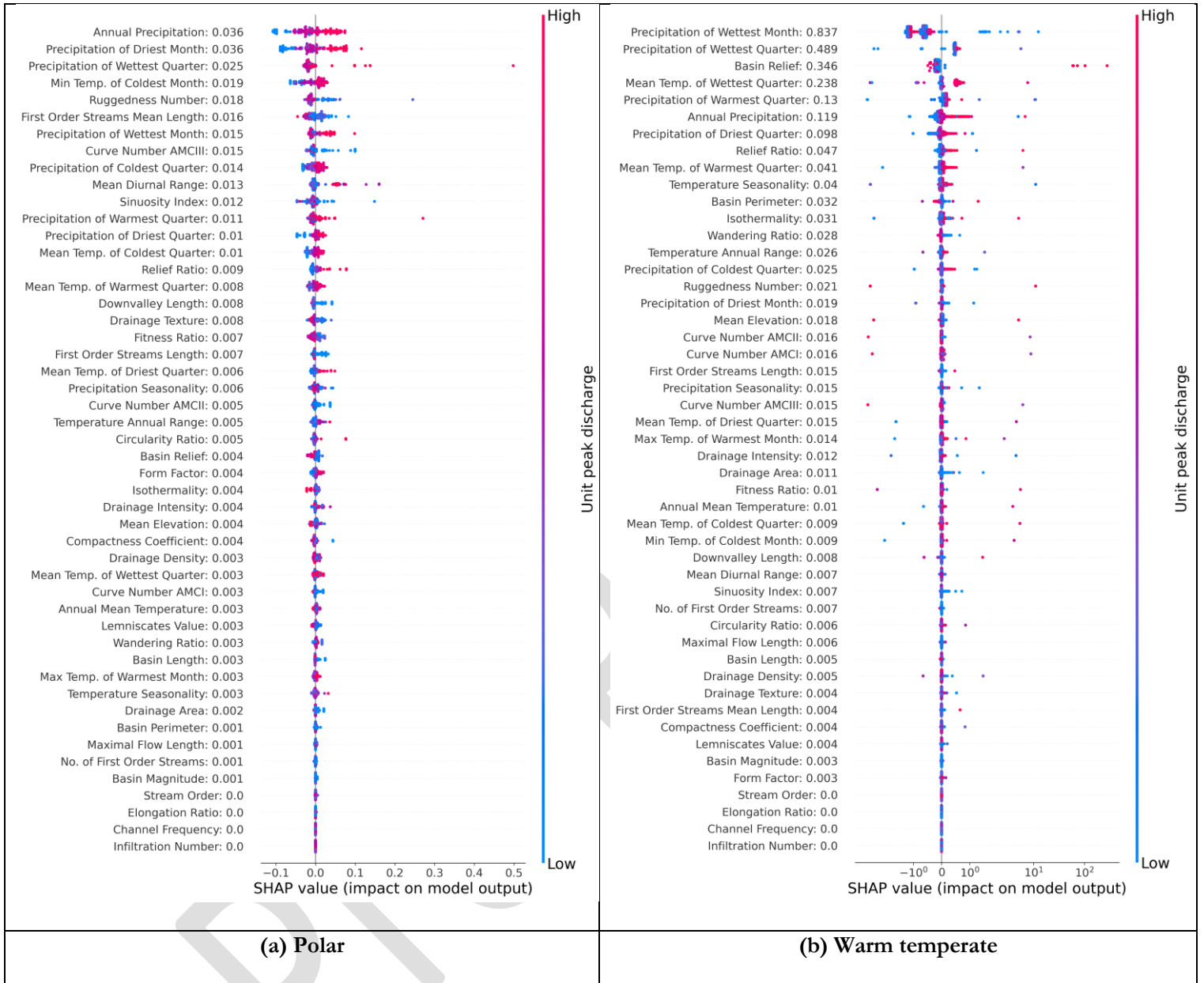
627 quarter, and basin relief are significantly top 3 dominant features over the remaining on
628 predicatnd – UPD of HSE. Moreover, it is observed that a few events corresponding to lower
629 values of precipitation of wettest month have a high positive impact on the model, while the
630 intermittent distribution of both higher and lower values on the negative side confirms that
631 there is likely another interaction at play beyond this variable, but in general as an aggregate
632 of all events it is the most influencing variable. At the same time, lower values of the
633 precipitation of wettest quarter corresponding to a few of the predicted target values have a
634 higher negative impact, but overall, the distribution confirms that this variable is positively
635 correlated with higher values having minimal impact on the target variable compared to other
636 features and as in case of an earlier noted lower values. In the case of basin relief, the higher
637 values have a high impact on both sides, while lower most of lower values are close to zero,
638 having not much impact. Higher values of the mean temperature of wettest quarter have a
639 positive impact on the model, while lower values have a negative impact, with most of them
640 being close to zero.

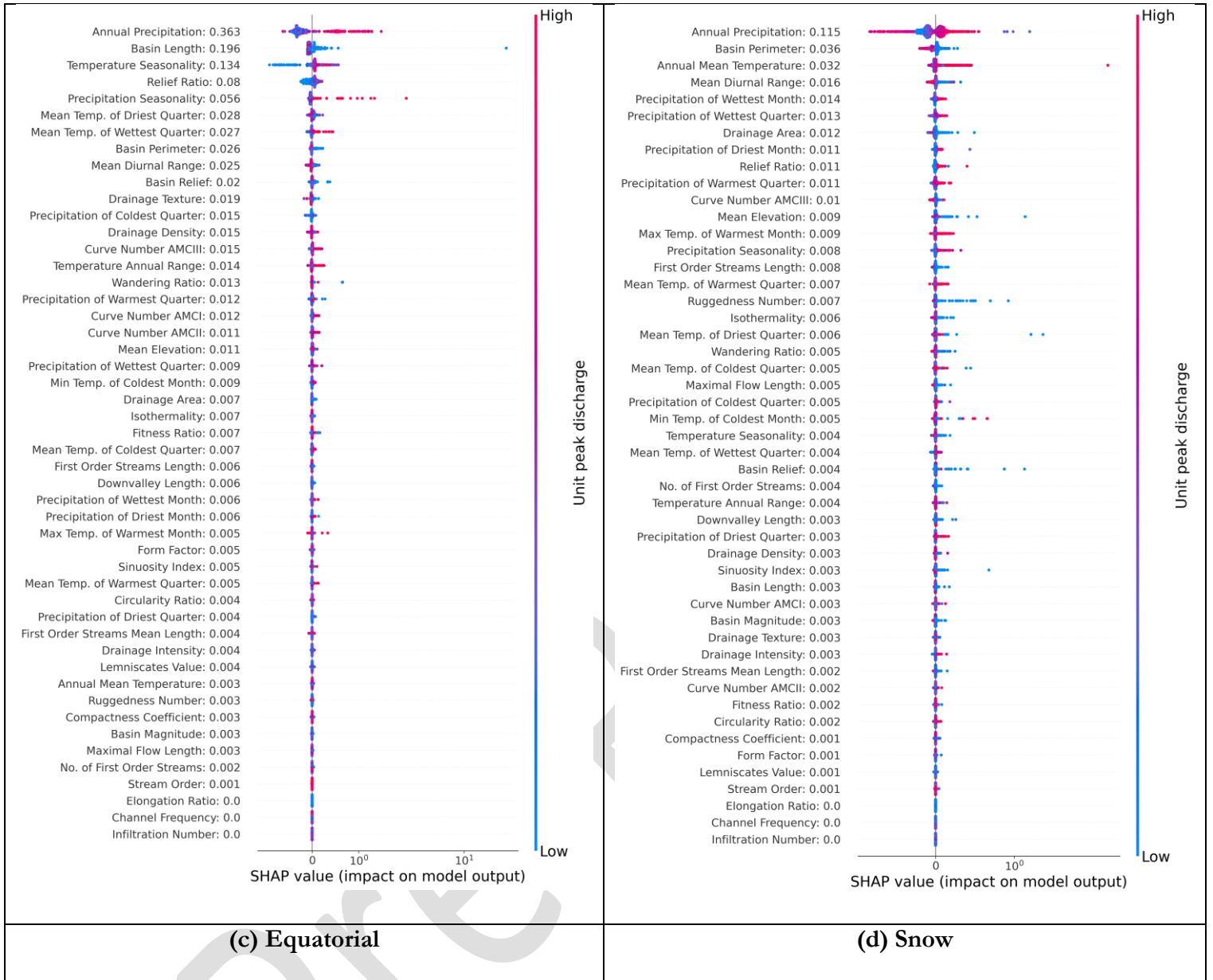
641 At the same time, in the case of equatorial dominated catchments, annual precipitation and
642 basin length are the top 2 influencing variables with a huge margin among others based on
643 the absolute mean of SHAP values for modeling UPD. Moreover, Figure 8(c) illustrates that
644 higher values of annual precipitation have a huge positive impact on the model output. In
645 contrast, lower basin length values have a positive impact compared to higher basin lengths,
646 as expected.

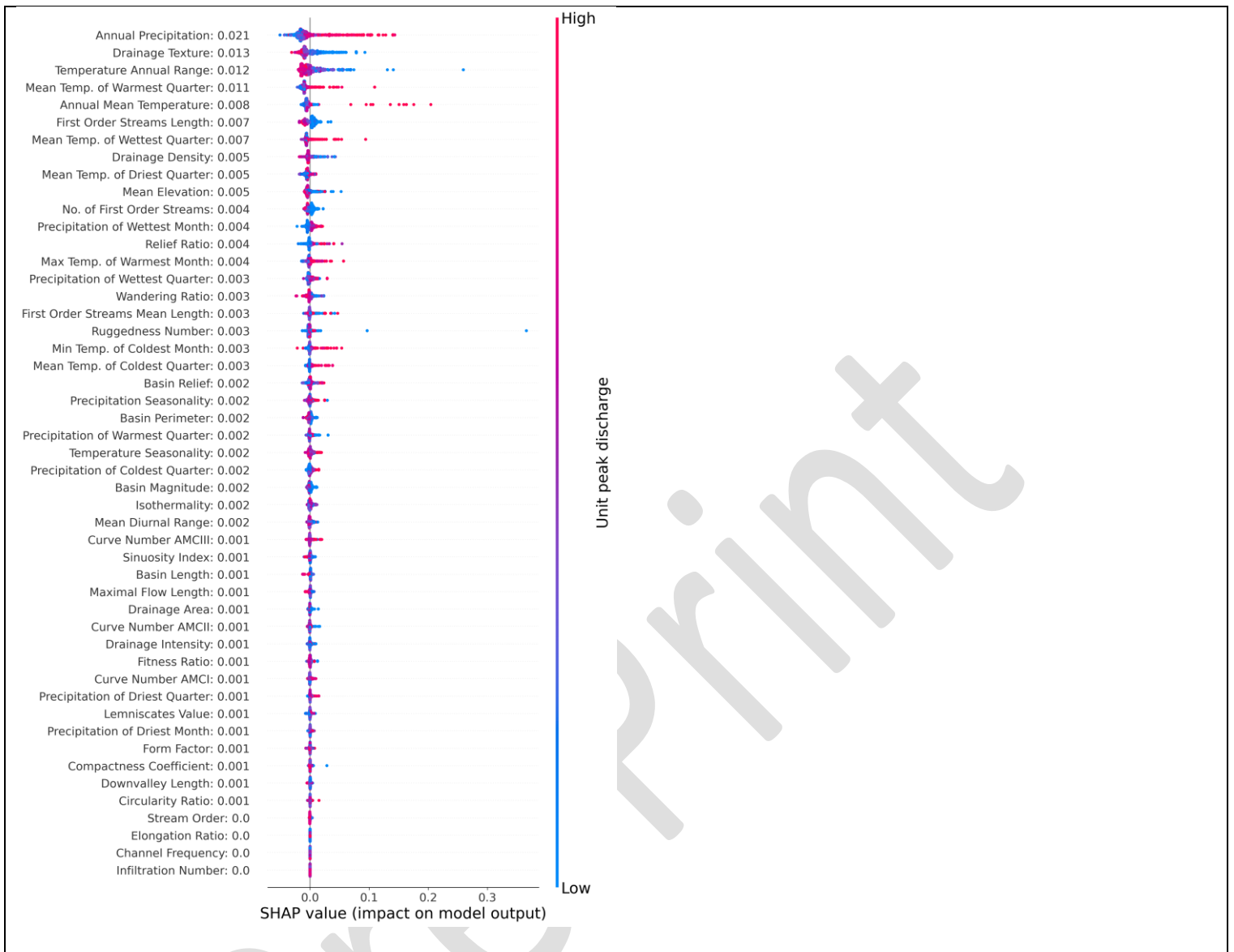
647 According to the SHAP summary plot of HSE events in Snow regions, annual precipitation,
648 basin perimeter, annual mean temperature, mean diurnal range, and precipitation of wettest
649 month are topmost five important variables for modeling. Besides, It is observed that most of
650 the high values of annual precipitation have a high impact in both directions showing a
651 likelihood of another interaction at play. In comparison, basin perimeter shows an evident

652 negative correlation with the target variable. Besides, higher annual mean temperature values
653 have a higher positive impact on the model, and lower values do not exhibit much impact on
654 the model. The mean absolute value of SHAP values of annual precipitation feature (0.115) is
655 observed to be three times its consecutive variable, showing it has significant influence over
656 the other variables among the top 5.

657 Finally, annual precipitation, drainage texture, temperature annual range, mean temperature
658 of warmest quarter, and annual mean temperature are the top 5 influencing features in the arid
659 catchments based on the SHAP summary plot as shown in Figure 8(e). Besides, it was
660 observed that the lower drainage texture values exhibit a high positive impact on the model
661 compared to the intensity of its higher values on the negative side. Similarly, the temperature
662 annual range also possesses the same characteristic in the model. In contrast, higher values of
663 the mean temperature of warmest quarter and annual mean temperature have a positive
664 impact on the model with great influence compared to its lower values, which have a negative
665 impact on the model.







(e) Arid

666 **Figure 8:** SHAP summary plots for different climatic classes. The order of the features along
 667 the y-axis are based on their importance in descending order. The value on the right side of
 668 the features name along the y-axis denotes mean absolute SHAP values for the corresponding
 669 features. The horizontal location of the dots depicts the intensity of its influence on
 670 predictions. Zero values on the x-axis indicate no impact, and positive (negative) values
 671 towards the rights (left) side indicate positive (negative) impact. The color of the dots
 672 represents the values of the corresponding features if it is high (red) or low (blue) for that
 673 observation in the dataset.

674 8. Conclusion

675 A database that allows for the characterization of streamflow extremes across the globe
 676 was built by using a spatially representative dataset of gauge observations combined with

677 catchment-averaged geographical attributes. With the objective to provide a broad overview
678 of a critical characteristic - unit peak discharge – of streamflow extremes across the world,
679 spatial and temporal distribution plots, boxplots, correlation plots, envelop curves, and a
680 machine learning approach (random forest model combined with SHAP) were employed
681 whose preliminary results are summarized as follows:

- 682 • It is found that, in general, meteorological variables have a larger correlation with the
683 UPD of HSE events compared to geomorphological variables. Among the
684 meteorological variables, annual precipitation, precipitation of wettest month and
685 quarter, precipitation of coldest quarter, precipitation of driest quarter and month
686 showed the highest correlations. For geomorphology, basin magnitude, first-order
687 streams length, basin perimeter, drainage area, stream order, drainage texture, and
688 elongation ratio are among the variables which displayed the highest correlation with
689 the UPD of HSE events.
- 690 • Catchments in the polar climates have high median and mean values of UPD of HSE
691 events, followed by warm temperate. In contrast, catchments in the arid region have
692 the lowest median and mean UPD values among catchments in other climates.
- 693 • It is observed that the UPD values of HSE events over the mountainous terrain along
694 the oceans are usually high across the world. In contrast, the UPD values of HSE
695 events are comparatively low on the leeward side along the mountain range. Besides,
696 across climatic zones, many of the catchments over which high UPDs are recorded are
697 dominated by forest and agricultural landcover in their catchments. Subsequently, a
698 combination of catchment characteristics is associated with these catchments
699 depicting a need in this study.

- 700 • The temporal distribution of most of the HSE events in the catchments dominated by
701 Polar climate are observed in summer. While in Arid climate catchments, most of the
702 HSE events over NH and SH are caused in May and June, and January to March,
703 respectively. Similarly, Snow climate catchments in the NH experience most HSE
704 events between April and June. Whereas, most of the HSE events in the catchments
705 dominated by Warm temperate climates are observed between December and
706 February at NH and SH. At the same time, over Equatorial catchments in NH and SH,
707 these extreme events are observed maximum from August to October and December
708 to March, respectively.
- 709 • Envelope curves over the global extremes were consistent with relationships
710 developed over continental United States and Europe in the existing studies. Besides,
711 the higher α value, i.e., the reduced discharge of the global sample, compared with
712 values reported for the continental United States and Europe, indicates that the
713 maximum magnitude of extremes across the globe is much higher than those reported
714 in their respective catchments. Moreover, the higher deviation value of β from zero in
715 the case of global events indicates the rate of change of UPD with change in drainage
716 area is faster than continental United States and Europe catchments.
- 717 • In General, catchments dominated by forests are observed to have high median values
718 of UPD of HSE events across the world. At the same time, catchments dominated by
719 mixed sedimentary rocks in polar climates, intermediate volcanic rocks in warm
720 temperate climates, pyroclastics, followed by basic volcanic rocks in equatorial
721 climates, Ice and glaciers, followed by basic plutonic type lithology in snow climates,
722 and intermediate volcanic rocks in arid catchments have a high median value of UPD
723 of HSE events in their respective climates among other catchments – covered with
724 different lithology types. The maximum median value of UPD corresponds to

725 cambisols in polar climates, fluvisols in warm temperate, vertisols in equatorial and
726 arid, and gleysols, followed by alisols soil type dominated catchments, among others
727 in their respective climates. These findings advise that catchments with these
728 characteristics generally have a high UPD in their respective climates. However, since
729 the resultant is a result of a multitude of variables, many other factors combinedly
730 come into play. Moreover, these ambiguous observations in this study highlight the
731 necessity for a more comprehensive study on how land features like landcover,
732 lithology, and soil type will influence the magnitude of high streamflow extremes or
733 floods.

734 • The random forest machine learning approach is relatively new in combination with
735 the SHAP interpretable approach. It is observed that meteorological variables,
736 especially annual precipitation, are the most influencing variable across the climatic
737 classes leaving warm temperate where precipitation of wettest month is the top
738 influencing one. The summary of most influencing variables in each climatic class are
739 as follows:

- 740 a. Polar: Annual precipitation, precipitation of driest month, precipitation of
741 wettest quarter, min. temperature of coldest month and ruggedness number
- 742 b. Warm Temperate: precipitation of wettest month, precipitation of wettest
743 quarter, and basin relief.
- 744 c. Equatorial: annual precipitation, and basin length
- 745 d. Snow: annual precipitation, basin perimeter, annual mean temperature, mean
746 diurnal range, and precipitation of wettest month.
- 747 e. Arid: annual precipitation, drainage texture, temperature annual range, mean
748 temperature of warmest quarter, and annual mean temperature.

749 Overall, a clear insight into the possible spectrum of unit peak discharge values is extracted
750 from these relationships to predict the unit peak discharge at ungauged stations from the
751 known catchment characteristics. These findings can also help assess the nature of extremes
752 in future climate scenarios, consequently implicating risk management methods.

753 Future studies could employ more sophisticated modeling techniques and information-
754 theoretic approaches to explore the relationships between basin attributes. The dataset
755 developed as a part of this study is expected to have a wide variety of applications in land
756 surface hydrology and encourages to development of similar datasets utilizing multiple global
757 datasets. This study lays the groundwork for testing fundamental hydrological theories and
758 empirical relationships by embracing data-driven science as the new paradigm in hydrology.

759 **Acknowledgements:**

760 This research was conducted in the HydroSense Lab (<https://hydrosense.iitd.ac.in/>) at the
761 Indian Institute of Technology Delhi. The authors acknowledge IIT Delhi High Performance
762 Computing facility for providing computational and storage resources. Manabendra Saharia
763 acknowledges the financial support for this research through an ISRO Space Technology
764 Cell grant (RP04139) and the IIT Delhi New Faculty Seed Grant. The authors would also
765 like to thank the handling editor and the anonymous reviewers for providing useful
766 comments which greatly improved the quality of this manuscript.

768 **Compliance with Ethical Standards**

769 The authors declare that they have no conflict of interest.

771 **Data Availability**

772
773 The database that supports the findings in this study is released publicly online: Global Flood
774 characterization (GloFlo) Database <https://doi.org/10.5281/zenodo.7158027>

775 The source datasets of the same database are derived from the following resources available
776 in the public domain:

- 777 • Global Streamflow Indices and Metadata Archive (GSIM):
778 <https://doi.org/10.1594/PANGAEA.887477>
- 779 • Global Distributed Basin Characteristics (GDBC):
780 <https://figshare.com/s/6cd00491b850bad716d7>
- 781 • Worldclim: <https://worldclim.org/data/worldclim21.html>

- 782 • Global Kopper-Geiger Climate classification: <http://koeppen-geiger.vu-wien.ac.at/present.htm>
 783 • GCN250, Global Curve Number dataset: <https://doi.org/10.6084/m9.figshare.7756202.v1>
 784 • Global Reservoir and Dam (GRanD), version 1:
 785 <https://sedac.ciesin.columbia.edu/data/set/grand-v1-dams-rev01>

786

787 **Bibliography**

- 788 Addor, N., Do, H. X., Alvarez-Garreton, C., Coxon, G., Fowler, K., & Mendoza, P. A. (2020). Large-
 789 sample hydrology: Recent progress, guidelines for new datasets and grand challenges.
 790 *Hydrological Sciences Journal*, 65(5), 712–725.
 791 <https://doi.org/10.1080/02626667.2019.1683182>
 792 Addor, N., Nearing, G., Prieto, C., Newman, A. J., Vine, N. L., & Clark, M. P. (2018). A Ranking of
 793 Hydrological Signatures Based on Their Predictability in Space. *Water Resources Research*,
 794 54(11), 8792–8812. <https://doi.org/10.1029/2018WR022606>
 795 Ahn, K.-H., & Merwade, V. (2016). Role of Watershed Geomorphic Characteristics on Flooding in
 796 Indiana, United States. *Journal of Hydrologic Engineering*, 21(2), 05015021.
 797 [https://doi.org/10.1061/\(ASCE\)HE.1943-5584.0001289](https://doi.org/10.1061/(ASCE)HE.1943-5584.0001289)
 798 ALLABY, M. A. (2008). Bifurcation ratio. In M. ALLABY (Ed.), *A Dictionary of Earth Sciences*. Oxford
 799 University Press.
 800 [https://www.oxfordreference.com/view/10.1093/acref/9780199211944.001.0001/acref-](https://www.oxfordreference.com/view/10.1093/acref/9780199211944.001.0001/acref-9780199211944-e-868)
 801 [9780199211944-e-868](https://www.oxfordreference.com/view/10.1093/acref/9780199211944.001.0001/acref-9780199211944-e-868)
 802 Al-Rawas, G. A., & Valeo, C. (2010). Relationship between wadi drainage characteristics and peak-
 803 flood flows in arid northern Oman. *Hydrological Sciences Journal*, 55(3), 377–393.
 804 <https://doi.org/10.1080/026266661003718318>
 805 Arnell, N. W., & Gosling, S. N. (2016). The impacts of climate change on river flood risk at the global
 806 scale. *Climatic Change*, 134(3), 387–401. <https://doi.org/10.1007/s10584-014-1084-5>
 807 Ashraf M. D., & Yasushi Y. (2008). Effect of Land Cover Changes on Flooding: Example from Greater
 808 Dhaka of Bangladesh | IJG:International Journal of Geoinformatics. *International Journal of*
 809 *Geoinformatics*, 4(1). <https://creativitycity-j.gsc.osaka-cu.ac.jp/IJG/article/view/604>
 810 Berghuijs, W. R., Harrigan, S., Molnar, P., Slater, L. J., & Kirchner, J. W. (2019). The Relative
 811 Importance of Different Flood-Generating Mechanisms Across Europe. *Water Resources*
 812 *Research*, 55(6), 4582–4593. <https://doi.org/10.1029/2019WR024841>
 813 Blöschl, G., Hall, J., Parajka, J., Perdigão, R. A. P., Merz, B., Arheimer, B., Aronica, G. T., Bilibashi, A.,
 814 Bonacci, O., Borga, M., Čanjevac, I., Castellarin, A., Chirico, G. B., Claps, P., Fiala, K., Frolova,
 815 N., Gorbachova, L., Gül, A., Hannaford, J., ... Živković, N. (2017). Changing climate shifts
 816 timing of European floods. *Science*, 357(6351), 588–590.
 817 <https://doi.org/10.1126/science.aan2506>
 818 Bonanno, E., Blöschl, G., & Klaus, J. (2021). Flow directions of stream-groundwater exchange in a
 819 headwater catchment during the hydrologic year. *Hydrological Processes*, 35(8), e14310.
 820 <https://doi.org/10.1002/hyp.14310>
 821 Booker, D. J., & Woods, R. A. (2014). Comparing and combining physically-based and empirically-
 822 based approaches for estimating the hydrology of ungauged catchments. *Journal of*
 823 *Hydrology*, 508, 227–239. <https://doi.org/10.1016/j.jhydrol.2013.11.007>
 824 Brebbia, C. A., & Katsifarakis, K. L. (2007). *River Basin Management IV*. WIT Press.
 825 Breiman, L. (2001). Random Forests. *Machine Learning*, 45(1), 5–32.
 826 <https://doi.org/10.1023/A:1010933404324>
 827 Cao, W., Sofia, G., & Tarolli, P. (2020). Geomorphometric characterisation of natural and
 828 anthropogenic land covers. *Progress in Earth and Planetary Science*, 7(1), 2.
 829 <https://doi.org/10.1186/s40645-019-0314-x>

- 830 Castellarin, A. (2007). Probabilistic envelope curves for design flood estimation at ungauged sites.
831 *Water Resources Research*, 43(4). <https://doi.org/10.1029/2005WR004384>
- 832 Chorley, R. J. (1957). Illustrating the Laws of Morphometry. *Geological Magazine*, 94(2), 140–150.
833 Scopus. <https://doi.org/10.1017/S0016756800068412>
- 834 Costa, J. E. (1987). Hydraulics and basin morphometry of the largest flash floods in the conterminous
835 United States. *Journal of Hydrology*, 93(3), 313–338. [https://doi.org/10.1016/0022-1694\(87\)90102-8](https://doi.org/10.1016/0022-1694(87)90102-8)
- 836
- 837 Crippen, J. R., & Bue, C. D. (1977). Maximum floodflows in the conterminous United States. *Water
838 Supply Papers - U.S. Geological Survey (USA)*. <https://agris.fao.org/agris-search/search.do?recordID=US7759757>
- 839
- 840 Degenhardt, F., Seifert, S., & Szymczak, S. (2019). Evaluation of variable selection methods for
841 random forests and omics data sets. *Briefings in Bioinformatics*, 20(2), 492–503.
842 <https://doi.org/10.1093/bib/bbx124>
- 843 Dethier, E. N., Sartain, S. L., Renshaw, C. E., & Magilligan, F. J. (2020). Spatially coherent regional
844 changes in seasonal extreme streamflow events in the United States and Canada since 1950.
845 *Science Advances*. <https://doi.org/10.1126/sciadv.aba5939>
- 846 Dijck, S. van. (2000). Effects of agricultural land use on surface runoff and erosion in a Mediterranean
847 area. *Nederlands Geografische Studies (Netherlands)*. <https://agris.fao.org/agris-search/search.do?recordID=NL2000003460>
- 848
- 849 Do, H. X., Westra, S., & Leonard, M. (2017). A global-scale investigation of trends in annual maximum
850 streamflow. *Journal of Hydrology*, 552, 28–43. <https://doi.org/10.1016/j.jhydrol.2017.06.015>
- 851 Do, H. X., Westra, S., Leonard, M., & Gudmundsson, L. (2020). Global-Scale Prediction of Flood
852 Timing Using Atmospheric Reanalysis. *Water Resources Research*, 56(1), e2019WR024945.
853 <https://doi.org/10.1029/2019WR024945>
- 854 Do, H. X., Zhao, F., Westra, S., Leonard, M., Gudmundsson, L., Boulange, J. E. S., Chang, J., Ciais, P.,
855 Gerten, D., Gosling, S. N., Müller Schmied, H., Stacke, T., Telteu, C.-E., & Wada, Y. (2020).
856 Historical and future changes in global flood magnitude – evidence from a model–
857 observation investigation. *Hydrology and Earth System Sciences*, 24(3), 1543–1564.
858 <https://doi.org/10.5194/hess-24-1543-2020>
- 859 Dormann, C. F., Elith, J., Bacher, S., Buchmann, C., Carl, G., Carré, G., Marquéz, J. R. G., Gruber, B.,
860 Lafourcade, B., Leitão, P. J., Münkemüller, T., McClean, C., Osborne, P. E., Reineking, B.,
861 Schröder, B., Skidmore, A. K., Zurell, D., & Lautenbach, S. (2013). Collinearity: A review of
862 methods to deal with it and a simulation study evaluating their performance. *Ecography*,
863 36(1), 27–46. <https://doi.org/10.1111/j.1600-0587.2012.07348.x>
- 864 Faniran, A. (1968). The index of drainage intensity—A provisional new drainage factor. *Aust J Sci*,
865 31(9), 328–330. Scopus.
- 866 Fick, S. E., & Hijmans, R. J. (2017). WorldClim 2: New 1-km spatial resolution climate surfaces for
867 global land areas. *International Journal of Climatology*, 37(12), 4302–4315.
868 <https://doi.org/10.1002/joc.5086>
- 869 Gaume, E., Bain, V., Bernardara, P., Newinger, O., Barbuc, M., Bateman, A., Blaškovičová, L., Blöschl,
870 G., Borga, M., Dumitrescu, A., Daliakopoulos, I., Garcia, J., Irimescu, A., Kohnova, S.,
871 Koutroulis, A., Marchi, L., Matreata, S., Medina, V., Preciso, E., ... Viglione, A. (2009). A
872 compilation of data on European flash floods. *Journal of Hydrology*, 367(1), 70–78.
873 <https://doi.org/10.1016/j.jhydrol.2008.12.028>
- 874 Gaume, E., & Borga, M. (2008). Post-flood field investigations in upland catchments after major flash
875 floods: Proposal of a methodology and illustrations. *Journal of Flood Risk Management*, 1(4),
876 175–189. <https://doi.org/10.1111/j.1753-318X.2008.00023.x>
- 877 Gourdol, L., Clément, R., Juilleret, J., Pfister, L., & Hissler, C. (2021). Exploring the regolith with
878 electrical resistivity tomography in large-scale surveys: Electrode spacing-related issues and
879 possibility. *Hydrology and Earth System Sciences*, 25(4), 1785–1812.
880 <https://doi.org/10.5194/hess-25-1785-2021>

- 881 Gravelius, H. (1914). *Flusskunde*. G.J. g??schen.
- 882 GREGORY, K. J., & WALLING, D. E. (1968). The Variation of Drainage Density Within a Catchment.
883 *International Association of Scientific Hydrology. Bulletin*, 13(2), 61–68.
884 <https://doi.org/10.1080/02626666809493583>
- 885 Gudmundsson, L., Do, H. X., Leonard, M., & Westra, S. (2018). *The Global Streamflow Indices and*
886 *Metadata Archive (GSIM) – Part 2: Quality control, time-series indices and homogeneity*
887 *assessment*. 18.
- 888 Gudmundsson, L., Leonard, M., Do, H. X., Westra, S., & Seneviratne, S. I. (2019). Observed Trends in
889 Global Indicators of Mean and Extreme Streamflow. *Geophysical Research Letters*, 46(2),
890 756–766. <https://doi.org/10.1029/2018GL079725>
- 891 Gupta, H. V., Perrin, C., Blöschl, G., Montanari, A., Kumar, R., Clark, M., & Andréassian, V. (2014).
892 Large-sample hydrology: A need to balance depth with breadth. *Hydrology and Earth System*
893 *Sciences*, 18(2), 463–477. <https://doi.org/10.5194/hess-18-463-2014>
- 894 Hall, J., Arheimer, B., Aronica, G. T., Bilibashi, A., Boháč, M., Bonacci, O., Borga, M., Burlando, P.,
895 Castellarin, A., Chirico, G. B., Claps, P., Fiala, K., Gaál, L., Gorbachova, L., Gül, A., Hannaford,
896 J., Kiss, A., Kjeldsen, T., Kohnová, S., ... Blöschl, G. (2015). A European Flood Database:
897 Facilitating comprehensive flood research beyond administrative boundaries. *Proceedings of*
898 *the International Association of Hydrological Sciences*, 370, 89–95.
899 <https://doi.org/10.5194/piahs-370-89-2015>
- 900 Hannaford, J., & Marsh, T. J. (2008). High-flow and flood trends in a network of undisturbed
901 catchments in the UK. *International Journal of Climatology*, 28(10), 1325–1338.
902 <https://doi.org/10.1002/joc.1643>
- 903 Hartmann, J., & Moosdorf, N. (2012). Global Lithological Map Database v1.0 (gridded to 0.5° spatial
904 resolution) [Data set]. In *Supplement to: Hartmann, Jens; Moosdorf, Nils (2012): The new*
905 *global lithological map database GLiM: A representation of rock properties at the Earth*
906 *surface. Geochemistry, Geophysics, Geosystems*, 13, Q12004,
907 <https://doi.org/10.1029/2012GC004370>. PANGAEA.
908 <https://doi.org/10.1594/PANGAEA.788537>
- 909 Hengl, T., Jesus, J. M. de, Heuvelink, G. B. M., Gonzalez, M. R., Kilibarda, M., Blagotić, A., Shangguan,
910 W., Wright, M. N., Geng, X., Bauer-Marschallinger, B., Guevara, M. A., Vargas, R., MacMillan,
911 R. A., Batjes, N. H., Leenaars, J. G. B., Ribeiro, E., Wheeler, I., Mantel, S., & Kempen, B.
912 (2017). SoilGrids250m: Global gridded soil information based on machine learning. *PLOS*
913 *ONE*, 12(2), e0169748. <https://doi.org/10.1371/journal.pone.0169748>
- 914 Hodgkins, G. A., Whitfield, P. H., Burn, D. H., Hannaford, J., Renard, B., Stahl, K., Fleig, A. K., Madsen,
915 H., Mediero, L., Korhonen, J., Murphy, C., & Wilson, D. (2017). Climate-driven variability in
916 the occurrence of major floods across North America and Europe. *Journal of Hydrology*, 552,
917 704–717. <https://doi.org/10.1016/j.jhydrol.2017.07.027>
- 918 Horton, R. E. (1932). Drainage-basin characteristics. *Transactions, American Geophysical Union*, 13,
919 350–361. <https://doi.org/10.1029/TR013i001p00350>
- 920 HORTON, R. E. (1945). EROSIONAL DEVELOPMENT OF STREAMS AND THEIR DRAINAGE BASINS;
921 HYDROPHYSICAL APPROACH TO QUANTITATIVE MORPHOLOGY. *GSA Bulletin*, 56(3), 275–
922 370. [https://doi.org/10.1130/0016-7606\(1945\)56\[275:EDOSAT\]2.0.CO;2](https://doi.org/10.1130/0016-7606(1945)56[275:EDOSAT]2.0.CO;2)
- 923 Huang, Y.-F., Tsang, Y., Strauch, A. M., & Clilverd, H. M. (2021). Shifting magnitude and timing of
924 streamflow extremes and the relationship with rainfall across the Hawaiian Islands. *Journal*
925 *of Hydrology*, 600, 126424. <https://doi.org/10.1016/j.jhydrol.2021.126424>
- 926 Ivancic, T. J., & Shaw, S. B. (2015). Examining why trends in very heavy precipitation should not be
927 mistaken for trends in very high river discharge. *Climatic Change*, 133(4), 681–693.
928 <https://doi.org/10.1007/s10584-015-1476-1>
- 929 Jaafar, H. H., Ahmad, F. A., & El Beyrouthy, N. (2019). GCN250, new global gridded curve numbers
930 for hydrologic modeling and design. *Scientific Data*, 6(1), 145.
931 <https://doi.org/10.1038/s41597-019-0155-x>

- 932 Jencso, K. G., & McGlynn, B. L. (2011). Hierarchical controls on runoff generation: Topographically
 933 driven hydrologic connectivity, geology, and vegetation. *Water Resources Research*, 47(11).
 934 <https://doi.org/10.1029/2011WR010666>
- 935 Kadoya, M. (1992). Study on Record Flood Peaks in Japan. *Proceedings of the Japan Academy, Series*
 936 *B*, 68(8), 133–138. <https://doi.org/10.2183/pjab.68.133>
- 937 Kiran, K. S., Bhuvaneshwari Devi, A., & Nair, A. M. (2017, December 11). Impact of Land Use Changes
 938 in a Micro Watershed using Remote Sensing and GIS: A Case Study of IIT Guwahati
 939 Watershed, Guwahati, Assam. *7th International Ground Water Conference*.
- 940 Kottek, M., Grieser, J., Beck, C., Rudolf, B., & Rubel, F. (2006). World Map of the Köppen-Geiger
 941 climate classification updated. *Meteorologische Zeitschrift*, 259–263.
 942 <https://doi.org/10.1127/0941-2948/2006/0130>
- 943 Kundzewicz, Z. W., Graczyk, D., Maurer, T., Pińskwar, I., Radziejewski, M., Svensson, C., & Szwed, M.
 944 (2005). Trend detection in river flow series: 1. Annual maximum flow / Détection de
 945 tendance dans des séries de débit fluvial: 1. Débit maximum annuel. *Hydrological Sciences*
 946 *Journal*, 50(5), null-810. <https://doi.org/10.1623/hysj.2005.50.5.797>
- 947 Kuntla, S. K. (2021). An era of Sentinels in flood management: Potential of Sentinel-1, -2, and -3
 948 satellites for effective flood management. *Open Geosciences*, 13(1), 1616–1642.
 949 <https://doi.org/10.1515/geo-2020-0325>
- 950 Land and Water Division. (2006). *Guidelines for soil description*. FAO.
 951 <http://www.fao.org/publications/card/en/c/903943c7-f56a-521a-8d32-459e7e0cdae9/>
- 952 Latrubesse, E. M., & Brea, D. (2009). Floods in Argentina. In E. M. Latrubesse (Ed.), *Developments in*
 953 *Earth Surface Processes* (Vol. 13, pp. 333–349). Elsevier. [https://doi.org/10.1016/S0928-](https://doi.org/10.1016/S0928-2025(08)10016-5)
 954 [2025\(08\)10016-5](https://doi.org/10.1016/S0928-2025(08)10016-5)
- 955 Lehner, B., Liermann, C. R., Revenga, C., Vörösmarty, C., Fekete, B., Crouzet, P., Döll, P., Endejan, M.,
 956 Frenken, K., & Magome, J. (2011). *Global Reservoir and Dam Database, Version 1*
 957 *(GRanDv1)*. <https://sedac.ciesin.columbia.edu/data/set/grand-v1-dams-rev01>
- 958 Linsley, R. K., Kohler, M. A., & Paulhus, J. L. H. (1949). *Applied Hydrology* (1st Ed Edition). McGraw
 959 Hill.
- 960 Lun, D., Viglione, A., Bertola, M., Komma, J., Parajka, J., Valent, P., & Blöschl, G. (2021).
 961 Characteristics and process controls of statistical flood moments in Europe – a data-based
 962 analysis. *Hydrology and Earth System Sciences*, 25(10), 5535–5560.
 963 <https://doi.org/10.5194/hess-25-5535-2021>
- 964 Lundberg, S., & Lee, S.-I. (2017). A Unified Approach to Interpreting Model Predictions.
 965 *ArXiv:1705.07874 [Cs, Stat]*. <http://arxiv.org/abs/1705.07874>
- 966 Lundberg, S. M., Erion, G., Chen, H., DeGrave, A., Prutkin, J. M., Nair, B., Katz, R., Himmelfarb, J.,
 967 Bansal, N., & Lee, S.-I. (2020). From local explanations to global understanding with
 968 explainable AI for trees. *Nature Machine Intelligence*, 2(1), 56–67.
 969 <https://doi.org/10.1038/s42256-019-0138-9>
- 970 Mallakpour, I., & Villarini, G. (2015). The changing nature of flooding across the central United
 971 States. *Nature Climate Change*, 5(3), 250–254. <https://doi.org/10.1038/nclimate2516>
- 972 Marchi, L., Borga, M., Preciso, E., & Gaume, E. (2010). Characterisation of selected extreme flash
 973 floods in Europe and implications for flood risk management. *Journal of Hydrology*, 394(1),
 974 118–133. <https://doi.org/10.1016/j.jhydrol.2010.07.017>
- 975 Melton, M. A. (1957). *An analysis of the relations among elements of climate, surface properties, and*
 976 *geomorphology*. New York : Department of Geology, Columbia University.
 977 <http://archive.org/details/analysisofrelati00melt>
- 978 Miller, O. M., & Summerson, C. H. (1960). Slope-Zone Maps. *Geographical Review*, 50(2), 194–202.
 979 <https://doi.org/10.2307/211507>
- 980 Miyaoka, K., Onodera, S., & Hirose, T. (1999). Effect of a permeable bedrock on runoff generation in
 981 steep mountainous catchments in the Kanto Mountains, Japan. *IAHS-AISH Publication*, 23–
 982 28. <http://pascal-francis.inist.fr/vibad/index.php?action=getRecordDetail&idt=1827974>

- 983 MUELLER, J. E. (1968). An Introduction to the Hydraulic and Topographic Sinuosity Indexes. *Annals of*
 984 *the Association of American Geographers*, 58(2), 371–385. [https://doi.org/10.1111/j.1467-](https://doi.org/10.1111/j.1467-8306.1968.tb00650.x)
 985 8306.1968.tb00650.x
- 986 Norbiato, D., Borga, M., Merz, R., Blöschl, G., & Carton, A. (2009). Controls on event runoff
 987 coefficients in the eastern Italian Alps. *Journal of Hydrology*, 375(3), 312–325.
 988 <https://doi.org/10.1016/j.jhydrol.2009.06.044>
- 989 O’Brian, R. (2020). *Eco-Hydromorphology – an emerging framework in river science* [University of
 990 Brighton]. https://cris.brighton.ac.uk/ws/portalfiles/portal/24457152/OBrian_Final.pdf
- 991 O’Connor, J. E., & Costa, J. E. (2004). Spatial distribution of the largest rainfall-runoff floods from
 992 basins between 2.6 and 26,000 km² in the United States and Puerto Rico. *Water Resources*
 993 *Research*, 40(1). <https://doi.org/10.1029/2003WR002247>
- 994 Owuor, S. O., Butterbach-Bahl, K., Guzha, A. C., Rufino, M. C., Pelster, D. E., Díaz-Pinés, E., & Breuer,
 995 L. (2016). Groundwater recharge rates and surface runoff response to land use and land
 996 cover changes in semi-arid environments. *Ecological Processes*, 5(1), 16.
 997 <https://doi.org/10.1186/s13717-016-0060-6>
- 998 Pal, S., Dominguez, F., Dillon, M. E., Alvarez, J., Garcia, C. M., Nesbitt, S. W., & Gochis, D. (2021).
 999 Hydrometeorological Observations and Modeling of an Extreme Rainfall Event Using WRF
 1000 and WRF-Hydro during the RELAMPAGO Field Campaign in Argentina. *Journal of*
 1001 *Hydrometeorology*, 22(2), 331–351. <https://doi.org/10.1175/JHM-D-20-0133.1>
- 1002 Peters-Lidard, C. D., Clark, M., Samaniego, L., Verhoest, N. E. C., van Emmerik, T., Uijlenhoet, R.,
 1003 Achieng, K., Franz, T. E., & Woods, R. (2017). Scaling, similarity, and the fourth paradigm for
 1004 hydrology. *Hydrology and Earth System Sciences*, 21(7), 3701–3713.
 1005 <https://doi.org/10.5194/hess-21-3701-2017>
- 1006 Project team ECA&D, & Royal Netherlands Meteorological Institute KNMI. (2013). *Algorithm*
 1007 *Theoretical Basis Document (ATBD)*. <https://www.ecad.eu/documents/atbd.pdf>
- 1008 Saharia, M., Kirstetter, P.-E., Vergara, H., Gourley, J. J., & Hong, Y. (2017). Characterization of floods
 1009 in the United States. *Journal of Hydrology*, 548, 524–535.
 1010 <https://doi.org/10.1016/j.jhydrol.2017.03.010>
- 1011 Saharia, M., Kirstetter, P.-E., Vergara, H., Gourley, J. J., Hong, Y., & Giroud, M. (2017). Mapping Flash
 1012 Flood Severity in the United States. *Journal of Hydrometeorology*, 18(2), 397–411.
 1013 <https://doi.org/10.1175/JHM-D-16-0082.1>
- 1014 Schumm, S. A. (1956). EVOLUTION OF DRAINAGE SYSTEMS AND SLOPES IN BADLANDS AT PERTH
 1015 AMBOY, NEW JERSEY. *GSA Bulletin*, 67(5), 597–646. [https://doi.org/10.1130/0016-](https://doi.org/10.1130/0016-7606(1956)67[597:EODSAS]2.0.CO;2)
 1016 7606(1956)67[597:EODSAS]2.0.CO;2
- 1017 Seneviratne, S. I., Nicholls, N., Easterling, D., Goodess, C. M., Kanae, S., Kossin, J., Luo, Y., Marengo,
 1018 J., McInnes, K., Rahimi, M., Reichstein, M., Sorteberg, A., Vera, C., Zhang, X., Rusticucci, M.,
 1019 Semenov, V., Alexander, L. V., Allen, S., Benito, G., ... Zwiers, F. W. (2012). Changes in Climate
 1020 Extremes and their Impacts on the Natural Physical Environment. In C. B. Field, V. Barros, T.
 1021 F. Stocker, & Q. Dahe (Eds.), *Managing the Risks of Extreme Events and Disasters to Advance*
 1022 *Climate Change Adaptation* (pp. 109–230). Cambridge University Press.
 1023 <https://doi.org/10.1017/CBO9781139177245.006>
- 1024 Shapley, L. S. (1953). 17. A Value for n-Person Games. In *17. A Value for n-Person Games* (pp. 307–
 1025 318). Princeton University Press. <https://doi.org/10.1515/9781400881970-018>
- 1026 Shen, X., Vergara, H. J., Nikolopoulos, E. I., Anagnostou, E. N., Hong, Y., Hao, Z., Zhang, K., & Mao, K.
 1027 (2016). GDBC: A tool for generating global-scale distributed basin morphometry.
 1028 *Environmental Modelling & Software*, 83, 212–223.
 1029 <https://doi.org/10.1016/j.envsoft.2016.05.012>
- 1030 Smart, J. S., & Surkan, A. J. (1967). The relation between mainstream length and area in drainage
 1031 basins. *Water Resources Research*, 3(4), 963–974. Scopus.
 1032 <https://doi.org/10.1029/WR003i004p00963>

- 1033 Stein, L., Clark, M. P., Knoben, W. J. M., Pianosi, F., & Woods, R. A. (2021). How Do Climate and
 1034 Catchment Attributes Influence Flood Generating Processes? A Large-Sample Study for 671
 1035 Catchments Across the Contiguous USA. *Water Resources Research*, 57(4), e2020WR028300.
 1036 <https://doi.org/10.1029/2020WR028300>
- 1037 Stein, L., Pianosi, F., & Woods, R. (2020). Event-based classification for global study of river flood
 1038 generating processes. *Hydrological Processes*, 34(7), 1514–1529.
 1039 <https://doi.org/10.1002/hyp.13678>
- 1040 STRAHLER, A. N. (1952). DYNAMIC BASIS OF GEOMORPHOLOGY. *GSA Bulletin*, 63(9), 923–938.
 1041 [https://doi.org/10.1130/0016-7606\(1952\)63\[923:DBOG\]2.0.CO;2](https://doi.org/10.1130/0016-7606(1952)63[923:DBOG]2.0.CO;2)
- 1042 STRAHLER, A. N. (1964). *Quantitative Geomorphology of Drainage Basins and Channel Networks*.
 1043 McGraw Hill.
- 1044 Subramanya, K. (1984). *Engineering Hydrology* (2nd ed.). McGraw Hill.
- 1045 Svensson, C., Kundzewicz, W. Z., & Maurer, T. (2005). Trend detection in river flow series: 2. Flood
 1046 and low-flow index series / Détection de tendance dans des séries de débit fluvial: 2. Séries
 1047 d'indices de crue et d'étiage. *Hydrological Sciences Journal*, 50(5), null-824.
 1048 <https://doi.org/10.1623/hysj.2005.50.5.811>
- 1049 *The Climate Change Initiative Land Cover (CCI-LC)*. (n.d.). ESA/CCI Viewer. Retrieved April 15, 2022,
 1050 from <https://maps.elie.ucl.ac.be/CCI/viewer/>
- 1051 Wang, F., Wang, Y., Zhang, K., Hu, M., Weng, Q., & Zhang, H. (2021). Spatial heterogeneity modeling
 1052 of water quality based on random forest regression and model interpretation.
 1053 *Environmental Research*, 202, 111660. <https://doi.org/10.1016/j.envres.2021.111660>
- 1054 Wang, S., Peng, H., & Liang, S. (2022). Prediction of estuarine water quality using interpretable
 1055 machine learning approach. *Journal of Hydrology*, 605, 127320.
 1056 <https://doi.org/10.1016/j.jhydrol.2021.127320>
- 1057 Wasko, C., Nathan, R., & Peel, M. C. (2020). Trends in Global Flood and Streamflow Timing Based on
 1058 Local Water Year. *Water Resources Research*, 56(8), e2020WR027233.
 1059 <https://doi.org/10.1029/2020WR027233>
- 1060 Winsemius, H. C., Aerts, J. C. J. H., van Beek, L. P. H., Bierkens, M. F. P., Bouwman, A., Jongman, B.,
 1061 Kwadijk, J. C. J., Ligtvoet, W., Lucas, P. L., van Vuuren, D. P., & Ward, P. J. (2016). Global
 1062 drivers of future river flood risk. *Nature Climate Change*, 6(4), 381–385.
 1063 <https://doi.org/10.1038/nclimate2893>
- 1064 Wolman, M. G., & Miller, J. P. (1960). Magnitude and Frequency of Forces in Geomorphic Processes.
 1065 *The Journal of Geology*, 68(1), 54–74. <https://doi.org/10.1086/626637>
- 1066 Woltemade, C. J., Hawkins, T. W., Jantz, C., & Drzyzga, S. (2020). Impact of Changing Climate and
 1067 Land Cover on Flood Magnitudes in the Delaware River Basin, USA. *JAWRA Journal of the*
 1068 *American Water Resources Association*, 56(3), 507–527. <https://doi.org/10.1111/1752-1688.12835>
- 1070 Zhang, X. S., Amirthanathan, G. E., Bari, M. A., Laugesen, R. M., Shin, D., Kent, D. M., MacDonald, A.
 1071 M., Turner, M. E., & Tuteja, N. K. (2016). How streamflow has changed across Australia since
 1072 the 1950s: Evidence from the network of hydrologic reference stations. *Hydrology and Earth*
 1073 *System Sciences*, 20(9), 3947–3965. <https://doi.org/10.5194/hess-20-3947-2016>
- 1074

1075 **Appendix**

1076 **Table A1:** Climate formula of Koppen-Geiger for the main climates (Kottek et al., 2006).
 1077 Where, T_{max} and T_{min} are the monthly mean temperatures of the warmest and coldest
 1078 months, respectively. P_{ann} is the accumulated annual precipitation. P_{th} is a dryness threshold
 1079 in mm, which depends on $\{T_{ann}\}$, the absolute measure of the annual mean temperature in
 1080 °C, and on the annual cycle of precipitation: $P_{th} = 2\{T_{ann}\}$ if at least 2/3 of the annual
 1081 precipitation occurs in winter; $P_{th} = 2\{T_{ann}\} + 28$ if at least 2/3 of the annual precipitation
 1082 occurs in summer; $P_{th} = 2\{T_{ann}\} + 14$ otherwise.

Climate	Criterion
Polar	$T_{max} < +10$ °C
Warm Temperate	-3 °C $< T_{min} < +18$ °C
Equatorial	$T_{min} \geq +18$ °C
Snow	$T_{min} \leq -3$ °C
Arid	$P_{ann} < 10 P_{th}$

1083

1084

1085 **Table A2:** List of all the catchment characteristics considered in this study.

Catchment Characteristics	Description	Reference
Geomorphology		
Stream order (SO)	Strahler stream order, numerical measure of river's branching complexity	(STRAHLER, 1952)
Drainage area (DA)	The surface area of the catchment	
Basin magnitude (B.M.)	The number of first order streams	(Melton, 1957)
First order streams length (1SL)	The total length of first order streams	(HORTON, 1945)
Maximal flow length (MFL)	the length along the longest watercourse from the mouth to the head of the channel	(MUELLER, 1968)
Down valley length (DVL)	The straight distance from the river cell of interest to the basin mouth	(MUELLER, 1968)
Basin relief (B.R.)	The elevation difference between the highest point on the drainage divide and the mouth	(Costa, 1987)
Basin length (B.L.)	The maximal length of the line from a basin mouth to a point on the perimeter equidistant from the basin mouth in either direction around the perimeter	(GREGORY & WALLING, 1968)
Basin perimeter (B.P.)	The outer boundary of the watershed that enclosed its area	(Schumm, 1956)
First order streams mean length (1SML)	Mean length of first order streams. $1SML = 1SL/BM$	(STRAHLER, 1964)
Sinuosity index (SI)	$SI = MFL/DVL$	(Wolman & Miller, 1960)
Form factor (FF)	$FF = DA/BL^2$	(HORTON,

		1945)
Relief ratio (RR)	$RR = BR/BL$	(Schumm, 1956)
Elongation ratio (ER)	$ER = 2/(BL \times (DA/\pi)^{0.5})$	(Schumm, 1956)
Circularity ratio (CR)	$CR = 4 \pi DA/BP^2$	(Miller & Summerson, 1960)
Lemniscate value (LV)	$LV = BL^2/DA$	(Chorley, 1957)
Drainage texture (D.T.)	D.T. = Total number of streams of all order/B.P	(HORTON, 1945)
Drainage density (D.D.)	D.D. = Total length of streams of all order/DA	(HORTON, 1945)
Compactness coefficient (CC)	$CC = 0.2841 (BP/DA)^{0.5}$	(Gravelius, 1914)
Wandering ratio (W.R.)	MFL/BL	(Smart & Surkan, 1967)
Fitness ratio (F.R.)	MFL/BP	(Melton, 1957)
Channel frequency (CF)	CF = Total number of streams of all order/DA	(Horton, 1932)
Drainage intensity (DI)	CF/DD	(Faniran, 1968)
Infiltration number (IN)	CF x DD	(Faniran, 1968)
Ruggedness number (R.N.)	B.R. x D.D.	(STRAHLER, 1964)
Mean elevation (M.E.)	Mean elevation of the catchment	
Climatological/Meteorological		
Annual mean temperature (Bio1)	The annual mean temperature	(Fick & Hijmans, 2017)
Mean diurnal range (Bio2)	The mean of the monthly temperature ranges (monthly maximum minus monthly minimum)	
Isothermality (Bio3)	Isothermality quantifies how large the day-to-night temperatures oscillate relative to the summer-to-winter (annual) oscillations. $Bio3 = (Bio2/Bio7) \times 100$	
Temperature seasonality (Bio4)	The amount of temperature variation over a given year (or averaged years) based on the standard deviation (variation) of monthly temperature averages.	
Maximum temperature of warmest month (Bio5)	The maximum monthly temperature occurrence over a given year (time-series) or averaged span of years (normal).	
Minimum temperature of coldest month (Bio6)	The minimum monthly temperature occurrence over a given year (time-series) or averaged span of years (normal).	
Temperature annual range (Bio7)	A measure of temperature variation over a given period. $Bio7 = Bio5 - Bio6$	
Mean temperature of wettest Quarter (Bio8)	This quarterly index approximates mean temperatures that prevail during the wettest season.	
Mean temperature of driest quarter (Bio9)	This quarterly index approximates mean temperatures that prevail during the driest quarter.	
Mean temperature of warmest quarter (Bio10)	This quarterly index approximates mean temperatures that prevail during the warmest	

	quarter.	
Mean temperature of coldest quarter (Bio11)	This quarterly index approximates mean temperatures that prevail during the coldest quarter.	
Annual precipitation (Bio12)	This is the sum of all total monthly precipitation values.	
Precipitation of wettest month (Bio13)	This index identifies the total precipitation that prevails during the wettest month.	
Precipitation of driest month (Bio14)	This index identifies the total precipitation that prevails during the driest month.	
Precipitation seasonality (Bio15)	This is a measure of the variation in monthly precipitation totals over the course of the year. This index is the ratio of the standard deviation of the monthly total precipitation to the mean monthly total precipitation (also known as the coefficient of variation) and is expressed as a percentage.	
Precipitation of wettest quarter (Bio16)	This quarterly index approximates total precipitation that prevails during the wettest quarter.	
Precipitation of driest quarter (Bio17)	This quarterly index approximates total precipitation that prevails during the driest quarter.	
Precipitation of warmest quarter (Bio18)	This quarterly index approximates total precipitation that prevails during the warmest quarter.	
Precipitation of coldest quarter (Bio19)	This quarterly index approximates total precipitation that prevails during the coldest quarter.	
Other catchment characteristics		
Climate type	catchment climate (major groups of Koppen-Geiger system) if one Climate type present over more than 50% catchment area, otherwise 'No dominant class'.	(Kottek et al., 2006)
Land cover	catchment land -cover (U.N. Classification System for 2015) if one single land -cover type present over more than 50% catchment area, otherwise 'No dominant class'.	<i>(The Climate Change Initiative Land Cover (CCI-LC), n.d.)</i>
Lithology type	catchment lithology if one single lithology type present over more than 50% catchment area, otherwise 'No dominant class'.	(Hartmann & Moosdorf, 2012)
Soil type	catchment soil class (WRB) if one single soil class present over more than 50% catchment area, otherwise 'No dominant class'.	(Hengl et al., 2017)
Curve number for antecedent moisture conditions-I (dry)	An empirical parameter based on dry antecedent runoff conditions for predicting the runoff and infiltration due to a rainfall event.	(Jaafar et al., 2019)
Curve number for antecedent moisture conditions-II (average)	An empirical parameter based on average antecedent runoff conditions for predicting the runoff and infiltration due to a rainfall event.	

Curve number for antecedent moisture conditions-III (wet)	An empirical parameter based on wet antecedent runoff conditions for predicting the runoff and infiltration due to a rainfall event.	
---	--	--

1086

Pre-Print